Snowpack Changes in the Hindu Kush–Karakoram–Himalaya from CMIP5 Global Climate Models

SILVIA TERZAGO, JOST VON HARDENBERG, ELISA PALAZZI, AND
ANTONELLO PROVENZALE

Institute of Atmospheric Sciences and Climate, National Research Council, Turin, Italy

(Manuscript received 26 November 2013, in final form 18 July 2014)

ABSTRACT

The Hindu Kush, Karakoram, and Himalaya (HKKH) mountain ranges feed the most important Asian river systems, providing water to about 1.5 billion people. As a consequence, changes in snow dynamics in this area could severely impact water availability for downstream populations. Despite their importance, the amount, spatial distribution, and seasonality of snow in the HKKH region are still poorly known, owing to the limited availability of surface observations in this remote and high-elevation area. This work considers global climate models (GCM) participating in phase 5 of the Coupled Model Intercomparison Project (CMIP5) and analyzes how they represent current and future snowpack in the HKKH region in terms of snow depth and snow water equivalent. It is found that models with high spatial resolution (up to 1.25°) simulate a spatial pattern of the winter snowpack in greater agreement with each other, with observations, with reanalysis datasets, and with the orographic features of the region, compared to most lower-resolution models. The seasonal cycle of snow depth displays a unimodal regime, with a maximum in February–March and almost complete melting in summer. The models generally indicate thicker [in Hindu Kush–Karakoram (HKK)] or comparable (in the Himalayas) snow depth and higher snow water equivalent compared to the reanalyses for the control period 1980–2005. Future projections, evaluated in terms of the ensemble mean of GCM simulations, indicate a significant reduction in the spatial average of snow depth over the HKK and an even stronger decrease in the Himalayas, where a reduction between 25% and 50% is expected by the end of the twenty-first century.

1. Introduction

The Hindu Kush, Karakoram, and Himalaya (HKKH) region extends through Afghanistan, Bangladesh, Bhutan, China, India, Myanmar, Nepal, and Pakistan. Together with the Tibetan Plateau, it represents the largest mountain range in the world, including all 14 of the highest peaks above 8000 m (Yao et al. 2007). The water melt from snowpack in this region ensures a permanent water flow to the major Asian river systems, providing water for 1.5 billion people living downstream (Yao et al. 2012). The contribution of snow and glacier melt to the streamflow varies across the region, and it becomes essential in areas that receive little summer precipitation, such as the Hindu Kush–Karakoram (HKK) and the western Himalayas (Liniger et al. 1998; Bookhagen and Burbank 2010).

For these reasons, current and future environmental changes in the HKKH, in particular those affecting glaciers and snowpack, can have important effects on water availability to downstream populations and may influence their social and economic development. However, the characterization of climatic conditions in the HKKH in terms of temperature and especially precipitation, including their temporal and spatial variability and their influence on the snowpack and glacier dynamics, is still affected by severe uncertainties, owing to the remoteness of this area, to its complex orography, and to the limited availability of surface observations (Palazzi et al. 2013). As for cryospheric resources, several studies indicate that most Himalayan glaciers are retreating (Kääb et al. 2012; Bolch et al. 2012), while in the Hindu Kush, Karakoram, and northwestern Himalaya regions some glaciers have been stable or slightly advancing (Hewitt 2005; Bishop et al. 2008; Hewitt 2011; Gardelle et al. 2012;

Corresponding author address: Silvia Terzago, Institute of Atmospheric Sciences and Climate (ISAC-CNR), Corso Fiume 4, 10133 Turin, Italy.
E-mail: s.terzago@isac.cnr.it

Sarikaya et al. 2012). The physical processes and the dynamics that lead to these different responses are still insufficiently known (Bolch et al. 2012).

The HKKH mountains act as an orographic barrier that forces air masses to rise and cool, leading to water vapor condensation and producing precipitation in the form of rain or snow. There are two main dynamical mechanisms bringing humidity to the HKKH: the summer Indian monsoon and the western weather patterns (WWP), which act in different periods of the year and in different portions of the whole region. The Indian monsoon transports warm and moist air from the Indian Ocean northward, producing heavy precipitation over the southern slopes of the Himalayas during the summer months, from July to September. The WWP are weather disturbances coming from the Mediterranean and Caspian Seas and propagating eastward, mainly during winter months (Singh et al. 1995; Archer and Fowler 2004; Syed et al. 2006), which discharge precipitation over the HKK mountains, feeding the snow reservoirs.

The spatial and temporal distribution of precipitation in HKKH has been studied by Palazzi et al. (2013) using station-based gridded observations and satellite measurements, together with reanalysis and model data. That study highlighted the difficulty of considering any observational dataset as a reference for precipitation in this area and the consequent need for merging the different precipitation sources, considering their uncertainties and strengths. Other studies used meteorological data from in situ stations, mainly located in valley floors, to analyze the characteristics of precipitation in the HKKH region. For example, Archer and Fowler (2004) found statistically significant increases in winter, summer, and annual precipitation at several stations in the upper Indus basin (northern Pakistan) from about 1960 to 2000. Other studies, for example, Syed et al. (2006), investigated the effects of the North Atlantic Oscillation (NAO) and El Niño–Southern Oscillation (ENSO) on winter precipitation in central-southwestern Asia using an analysis of available observed climate data. The contribution of snowfall to total precipitation on the HKK and Himalaya slopes is still poorly known, owing to the scarcity of regular surface measurements, compared to more instrumented regions like the Tibetan Plateau. Singh et al. (1995), among others, studied the relationship between (solid and liquid) precipitation and elevation in the Chenab basin (western Himalayas), showing that the ratio of snowfall to the total annual precipitation increases linearly with elevation from about 15% to 75% in the range of 1300–4300 m above mean sea level (MSL). Winiger et al. (2005) analyzed the altitudinal variation of snow water equivalent (SNW; often referred to as SWE in the literature) measurements derived from several automatic weather stations in the Karakoram

and found that the contribution of snow to total precipitation can be as high as 90% at about 5000 m MSL.

A recent study considered a set of global climate model (GCM) simulations from phase 5 of the Coupled Model Intercomparison Project (CMIP5) and assessed their reliability in reproducing precipitation and temperature features over the Tibetan Plateau region (Su et al. 2013). They found that GCMs are able to capture reasonably well the climatological spatial pattern and variability of temperature, while all models tend to overestimate precipitation with respect to the observations. Only about half of the GCMs are able to reproduce the observed seasonal cycle of precipitation.

As for the analysis of snow-related variables, several papers have investigated the snowpack characteristics in the Tibetan Plateau region, for which in situ observations are available from the Chinese meteorological station network (You et al. 2011; Dahe et al. 2006; Qian et al. 2003; Wu and Qian 2003). Less attention has been focused on the Karakoram and Himalaya slopes, owing to sparse surface measurements with limited time coverage (Putkonen 2004; Winiger et al. 2005). In recent decades, however, satellite observations have allowed us to retrieve information on the extension and persistence of the snowpack, even in the less accessible/instrumented regions. For instance, Pu et al. (2007) analyzed the spatial distribution of snow cover over the Tibetan Plateau–HKKH regions using Moderate Resolution Imaging Spectroradiometer (MODIS) measurements and explored the seasonal cycle of the areal extension of snow cover. Similarly, Tahir et al. (2011) used MODIS data to study the variability of the snow cover extension in the upper Indus River basin (Karakoram Range, northern Pakistan). At a larger scale, Brutel-Vuilmet et al. (2013) investigated the areal extension of land snow cover in the Northern Hemisphere simulated by CMIP5 GCMs and found a good agreement between the models and the observations: the annual cycle of snow cover is correctly reproduced by the GCMs despite an underestimation of the amplitude of the trend of snow cover in spring.

From a hydrological point of view, in high-elevation areas such as the HKKH, the key parameters necessary to investigate the effects of climate change on the water cycle are the snow depth (SND) and the corresponding SNW, whose temporal and spatial variability, however, are still poorly known. A better knowledge of the snow climatology in this region would help to estimate the current and future availability of meltwater resources in southeastern Asia.

GCMs still have too coarse of a spatial resolution to reproduce the small-scale variability of precipitation and snowpack in orographically complex areas. Nevertheless,

they may be effective in providing, even at a regional scale, a smooth but coherent picture of the large-scale temporal and spatial patterns of snow cover and depth. The quantification of the uncertainties in GCM simulations is essential to define their skill in reproducing climate variability, to compare the historical model outputs with the available observed climatologies, to critically analyze future climate change projections of GCMs, and to provide fair information for policymakers to plan climate change mitigation and adaptation strategies.

In this paper, we investigate how the spatial and temporal variability of the snowpack in the HKKH region is represented in state-of-the-art GCMs participating in the CMIP5 effort by analyzing the historical and future behavior of their simulated SND and SNW quantities. We compare the model outputs in the historical period with the main, currently available SND and SNW datasets, including surface- and satellite-based observations and reanalysis data.

The paper is organized as follows. In section 2, we present the study area, the datasets used for the analysis, and the methodology employed for the data processing. In section 3, we discuss (i) the current snowpack characteristics in the HKKH region in terms of spatial distribution and of seasonal cycle, in observations, in reanalyses, and in GCM simulations and (ii) the changes detected in the historical period and expected by the end of the twenty-first century. Section 4 provides a summary and a general discussion of the results.

2. Data and methods

This study focuses on high-elevation areas of the HKKH region, where snow plays an important role for local climate, water resources, and ecosystems. The domain considered here is in the range 23°–39°N, 68°–105°E, as shown in Fig. 1. Owing to the different dominant circulations and precipitation regimes in the HKK and the Himalayas, we further divide the study area into two subregions: a northwestern area, prone to winter precipitation from the midlatitude disturbances carried by westerly winds, and a southeastern area, prone to heavy summer precipitation associated with the summer Indian monsoon. As in a previous study (Palazzi et al. 2013), we consider the HKK in the range 32°–37°N, 71°–78°E and the Himalayas in the range 25°–32°N, 78°–93°E.

We collected and analyzed the following datasets on snow depth and snow water equivalent, obtained from several sources:

- Global monthly Equal-Area Scalable Earth (EASE)-Grid snow water equivalent climatology (Armstrong
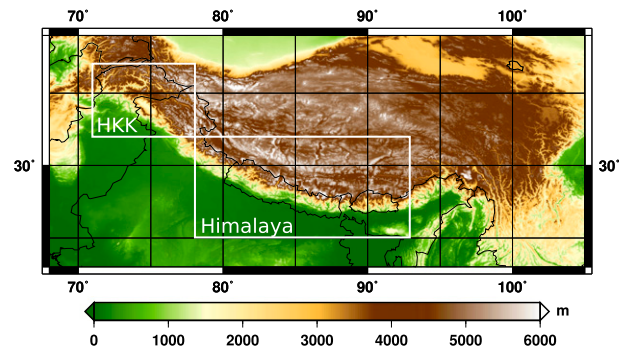

FIG. 1. Orography of the HKKH area (DEM from the GLOBE project). The white boxes represent the HKK and the Himalaya subregions considered in this study.

et al. 2005) provided by the National Snow and Ice Data Center (NSIDC). This dataset includes global, monthly satellite-derived snow water equivalent data from November 1978 through May 2007 at 25-km resolution. The snow water equivalent is derived from the Scanning Multichannel Microwave Radiometer (SMMR) and selected data from the Special Sensor Microwave Imager (SSM/I).

- Advanced Microwave Scanning Radiometer for Earth Observing System (AMSR-E)/*Aqua* monthly level 3 (L3) global snow water equivalent data (Tedesco et al. 2004) from the AMSR-E instrument on board the National Aeronautics and Space Administration (NASA) Earth Observing System *Aqua* satellite. This dataset contains SNW data and quality assurance flags mapped to 25-km EASE-Grids from 2002 to 2011.

- Daily snow depth analysis data (Brown and Brasnett 2010) by the Canadian Meteorological Centre (CMC), obtained from surface synoptic observations, meteorological aviation reports, and special aviation reports acquired from the World Meteorological Organization (WMO) information system. The data are gridded at a resolution of 24 km. This dataset includes daily observations and monthly means of both SND and SNW (estimated from SND using a density lookup table) from 1998 to 2011.

- Interim European Centre for Medium-Range Weather Forecasts (ECMWF) Re-Analysis (ERA-Interim)/Land, providing SND and SNW fields at ~0.7° spatial resolution (~67 km in the zonal direction) and covering the period 1979–2010 (Balsamo et al. 2013). ERA-Interim/Land is the result of offline simulations performed with the improved land surface model Hydrology-Tiled ECMWF Scheme for Surface Exchange over Land (HTESSEL) forced by the meteorological fields from ERA-Interim (Dee et al. 2011) and precipitation adjustments based on Global

Precipitation Climatology Project, version 2.1 (GPCP v2.1).

- Climate Forecast System Reanalysis (CFSR; Saha et al. 2010) by the National Centers for Environmental Prediction (NCEP): a global, high-resolution, coupled atmosphere–ocean–land surface–sea ice system reanalysis, covering the period 1979–2009 and providing, among other variables, SND and SNW fields at 0.3125° horizontal resolution (~30 km in the zonal direction).
- Twentieth Century Reanalysis, version 2 (20CRv2; Compo et al. 2011), provided by the National Oceanic and Atmospheric Administration (NOAA)/Earth System Research Laboratory (ESRL)/Physical Sciences Division and the Cooperative Institute for Research in Environmental Sciences (CIRES) Climate Diagnostics Center at the University of Colorado Boulder, containing a synoptic observation–based estimate of global tropospheric variability spanning the time period from 1871 to 2008. It is derived using only surface pressure observations and prescribing monthly SST and sea ice distributions as boundary conditions for the atmosphere (Compo et al. 2011). SND and SNW fields are available at ~1.875° spatial resolution (~180 km in the zonal direction).
- GCM simulations included in the CMIP5 archive (http://cmip-pcmdi.llnl.gov/cmip5/), as available in February 2014, that provide the snow depth and surface snow amount (corresponding to snow water equivalent) variables (Table 1) during both the historical (1850–2005) and projection (2006–2100) periods under the two representative concentration pathway (RCP) scenarios, RCP4.5 and RCP8.5 (Moss et al. 2010). Most modeling groups delivered data for either only snow depth (18 models) or for only snow water equivalent (7 models), while only 10 groups delivered both variables. As snow density is not among the variables archived by default in CMIP5, it is not possible to directly convert one variable into the other; thus, we consider them separately. In our analysis, we use data at monthly time scales. For each model, we use the ensemble member r1i1p1 when more than one ensemble member is available. We include in the ensemble also the EC-EARTH model (Hazeleger et al. 2012), for which the SND and SNW data were not stored in CMIP5, using the ensemble member r8i1p1 run by our institute. Among all CESM1-family models, we keep mainly CESM1 (BGC) for detailed analysis, since its data cover both the historical period and future projections in both RCP scenarios. The spatial resolution depends on the particular model and varies from 0.56° to 3.75° (~54–360 km in the zonal direction; see Table 1).

The datasets mentioned above are compared over the common time period 1980–2005 to investigate similarities and differences in the representation of the spatial distribution and characteristics of snowpack in the HKKH region. A realistic representation of snowpack in both GCMs and in reanalysis data is a very challenging task in such orographically complex areas because of the difficulty of representing the dominant physical processes of precipitation and snowpack dynamics on the coarse numerical grids used by the climate and reanalysis models. The use of reanalysis products in these regions should be considered with caution because of the scarcity of available meteorological observations, leading to few assimilated data and to model outputs that are poorly constrained by observations. Nevertheless, reanalysis products and GCM simulations are widely used in hydrological modeling chains and, consequently, for climate change impact studies. For this reason, it is important to assess their uncertainties and how these propagate across scales in the modeling chains. For example, Bao and Zhang (2013) verified that CFSR and ERA-Interim in the Tibetan Plateau show mean values of temperature and horizontal winds in good agreement with 3000 high-quality observations from a radiosonde network; on the other hand, the mean values of relative humidity show important biases relative to the observations. In a former study, Ma et al. (2009) compared precipitation fields from the previous versions of the ECMWF and NCEP reanalyses [i.e., the 40-yr ECMWF Re-Analysis (ERA-40) and the NCEP–U.S. Department of Energy (DOE) Atmospheric Model Intercomparison Project (AMIP-II) reanalysis] and from other gridded precipitation datasets [Climate Prediction Center Merged Analysis of Precipitation (CMAP) and GPCP] with station measurements over China, finding a poor agreement.

The new ERA-Interim/Land product employed in our study addresses the problem of the precipitation estimate by incorporating a precipitation bias correction based on the GPCP v2.1 data (Balsamo et al. 2013). The ERA-Interim/Land module HTESSEL, with respect to the previous version implemented in ERA-Interim [Tiled ECMWF Scheme for Surface Exchanges over Land (TESSEL); van den Hurk et al. 2000], includes a new snow scheme with improved estimates of snow density, representation of water storage in the snowpack, and interception (Balsamo et al. 2009; Dutra et al. 2010). ERA-Interim/Land preserves the closure of the water balance and it is therefore more suitable for climate applications than the original ERA-Interim dataset. Owing to the lack of surface measurements, snow density is not assimilated in ERA-Interim; thus, the estimate relies only on the capability of the land surface model to correctly reproduce the temporal variability of

snow cover (Balsamo et al. 2012). A validation study by Dutra et al. (2010) showed that, compared to meteorological stations and satellite data, the land surface model HTESSEL tends to underestimate both the extent of the snow-covered areas and the snow depth in winter and in early spring. Concerning CFSR and 20CRv2, as far as we know, the quality assessment of the snow products has not been carried out yet.

In this work we intercompare snow depth and snow water equivalent datasets provided by the CMIP5 GCMs, satellite sensors, surface analyses, and reanalyses. We analyze these datasets at their original spatial resolution, to avoid introducing additional artificial uncertainties related to spatial interpolation onto a common grid. To compare them, we use spatial averages with a "weighted mean" approach. First, as our focus is on the mountains, we define our areas of interest as those above 1000 m MSL using the 1-km spatial resolution Global Land One-km Base Elevation (GLOBE) digital elevation model (DEM; Hastings and Dunbar 1999). Then, we compute spatial averages over the HKKH subregions by weighting the original models/reanalyses grid values (at the native resolution) by the fraction of each grid cell falling in the selected subregion and with an elevation greater than 1000 m MSL in the high-spatial-resolution DEM. This procedure allows us to obtain spatial averages that are not biased by model grid size and to perform a fair comparison among models with different spatial resolutions.

3. Results

a. Spatial distribution of the snowpack

The seasonality of precipitation in the study area, with main contributions during winter in HKK and during summer in the Himalayas, suggests separate investigations of the cold [December–April (DJFMA)] and warm [June–September (JJAS)] seasons. To evaluate the current snowpack spatial distribution, we choose the period 1980–2005, in which data from most of the employed datasets are available, and focus our analysis on the snow depth and snow water equivalent variables. We initially consider all models, without establishing a priori any constraints on their use on the basis of their characteristics such as spatial resolution.

1) SNOW DEPTH

The snow depth variable is available for a larger number of models in CMIP5 (28 out of 35 considered in this work). Figure 2 shows the spatial distribution of the multiannual mean (1980–2005) of winter snow depth, obtained from the three reanalysis products, that is, ERA-Interim/Land, CFSR, and 20CRv2, and from

a representative subset of CMIP5 GCM historical simulations. The GCM maps are ordered according to the model grid size, from the highest to the lowest spatial resolution (see Table 1).

ERA-Interim/Land displays an artificial, fixed snow depth value of about 30 m over the Baltoro glacier (Karakoram): since this value is not intended to be representative of the real conditions, we exclude the corresponding area when comparing ERA-Interim/Land to the other reanalyses and to the GCM data [in Figs. 3, 5, 9, and Fig. 10 (top left); note that Figs. 3, 5, 9, and 10 are described in greater detail below]. Other peaks in snow depth are located in the Hindu Kush and Pamir mountains, northwest of the Karakoram, and in the western Himalayas. Snow depth decreases along the Himalayas toward the southeast direction and toward the Tibetan Plateau. The spatial pattern of snow depth is coherent with the observed mean winter temperatures in this area (Su et al. 2013): over the Tibetan Plateau, temperature generally shifts sharply from a few degrees above zero in the southeast of the Himalayas to less than $-18°C$ in the central and northwestern area of the Tibetan Plateau, with the lowest temperatures appearing in the central plateau and the northwest corner where elevations are generally above 5000 m MSL.

Excluding the Baltoro area, CFSR is in good agreement with ERA-Interim/Land, showing a very similar spatial pattern but slightly lower snow depth values. Compared to the former products, 20CRv2 presents higher snow depth in the western Himalayas, and nonnegligible snow depth in the eastern Himalayas and in the central Tibetan Plateau. The maximum values appear slightly shifted toward the Tibetan Plateau in 20CRv2 with respect to the other products, probably owing to the effect of its coarser spatial resolution and to the associated smooth orography.

When considering the models in CMIP5 with highest spatial resolution (in the range 0.56°–1.25°), shown in the second and third rows of Fig. 2, we see that they depict similar spatial patterns, with snow depth peaking over the HKK and decreasing toward the Himalayas and the Tibetan Plateau. The overall spatial distribution resembles that of the reanalyses, but the GCMs present slightly higher values; in particular, the MIROC4h GCM reports snow depth values up to 3 m in the highest-elevation areas. The other high-resolution GCMs generally provide thicker snow depth compared to ERA-Interim/Land and CFSR, and the magnitude of their maxima is more similar to 20CRv2. The high-resolution models indicate the presence of another snow depth peak in the southeastern part of the Tibetan Plateau, at the border with India, which is not found in ERA-Interim/Land but which appears (albeit with low amplitude) in the

TABLE 1. CMIP5 GCMs providing SND and/or SNW (d, SND only; w, SNW only; b, both) in the historical period. For each model the table specifies the corresponding land surface model (LSM), the spatial resolution of the stored fields in the zonal direction, and the spectral resolution or the Gaussian grid resolution of the model (if applicable). The high-spatial-resolution models highlighted in boldface have been used for the analysis of amplitude distributions and of the seasonal cycle of SND.

Acronym	Expansion	Institution	LSM	Spatial (°)/ spectral resolution	Reference
MIROC4h (d)	Model for Interdisciplinary Research on Climate (MIROC), version 4 (high resolution)	University of Tokyo	Minimal Advanced Treatments of Surface Interaction and Runoff (MATSIRO)	**0.5625**/T213	Sakamoto et al. (2012)
CMCC-CM (b)	Centro Euro-Mediterraneo per i Cambiamenti Climatici (CMCC) Climate Model	CMCC	ECHAM5	**0.75**/T159	Scoccimarro et al. (2011)
EC-EARTH (b)	EC-Earth Consortium	EC-Earth Consortium	HTESSEL	**1.125**/T159	Hazeleger et al. (2012)
BCC_CSM1.1(m) (b)	Beijing Climate Center (BCC), Climate System Model (CSM), version 1.1 (moderate resolution)	BCC	BCC Atmosphere and Vegetation Interaction Model, version 1.0 (BCC_AVIM1.0)	**1.125**/T106	Wu et al. (2013)
MRI-CGCM3 (d)	Meteorological Research Institute (MRI) Coupled Atmosphere–Ocean General Circulation Model, version 3	MRI	Hydrology, Atmosphere, and Land model (HAL)	**1.125**/T159	Yukimoto et al. (2012)
CESM1 (BGC) (b)	Community Earth System Model (CESM), version 1 (Biogeochemistry)	National Center for Atmospheric Research (NCAR)	Community Land Model, version 4 (CLM4)	**1.25**/—	Hurrell et al. (2013)
CESM1 (CAM5) (b)	CESM, version 1 [Community Atmosphere Model (CAM), version 5]	NCAR	CLM4	1.25/—	Hurrell et al. (2013)
CESM1 (FAST-CHEM) (b)	CESM, version 1 (with FASTCHEM)	NCAR	CLM4	1.25/—	Hurrell et al. (2013)
CCSM4 (b)	Community Climate System Model, version 4	NCAR	CLM4	1.25/—	Gent et al. (2011)
CNRM-CM5 (b)	Centre National de Recherches Météorologiques (CNRM) Coupled Global Climate Model, version 5	CNRM	Interactions between Soil, Biosphere, and Atmosphere (ISBA)	1.4/T127	Voldoire et al. (2013)
MIROC5 (d)	MIROC, version 5	University of Tokyo	MATSIRO	1.4/T85	Watanabe et al. (2010)
ACCESS1.0 (d)	Australian Community Climate and Earth-System Simulator, version 1.0	Commonwealth Scientific and Industrial Research Organisation (CSIRO)/ Bureau of Meteorology (BOM)	Met Office Surface Exchange Scheme 2 (MOSES 2)	1.875/N96	Bi et al. (2013)
CMCC-CMS (b)	CMCC Stratosphere-resolving Climate Model	CMCC	ECHAM5	1.875/T63	Scoccimarro et al. (2011)
CSIRO Mk3.6.0 (d)	CSIRO Mark 3.6.0	CSIRO	MOSES, version 2	1.875/T63	Collier et al. (2011)

TABLE 1. (*Continued*)

Acronym	Expansion	Institution	LSM	Spatial (°)/ spectral resolution	Reference
HadGEM2-CC (w)	Hadley Centre Global Environment Model (HadGEM), version 2 (Carbon Cycle)	Met Office Hadley Centre	MOSES, version 2	1.875/N96	Collins et al. (2011)
HadGEM2-ES (w)	HadGEM, version 2 (Earth System)	Met Office Hadley Centre	MOSES, version 2	1.875/N96	Collins et al. (2011)
MPI-ESM-LR (w)	Max Planck Institute (MPI) Earth System Model (ESM), low resolution	Max Planck Institute for Meteorology (MPI-M)	Jena Scheme for Biosphere–Atmosphere Coupling in Hamburg (JSBACH)	1.875/T63	Giorgetta et al. (2013)
MPI-ESM-MR (w)	MPI ESM, medium resolution	MPI-M	JSBACH	1.875/T63	Giorgetta et al. (2013)
MPI-ESM-P (w)	MPI ESM, paleo	MPI-M	JSBACH	1.875/T63	Giorgetta et al. (2013)
INM-CM4.0 (d)	Institute of Numerical Mathematics (INM) Coupled Model, version 4.0	INM	INM	2.0/—	Volodin et al. (2010)
CESM1 (WACCM) (d)	CESM, version 1 (Whole Atmosphere Community Climate Model)	NCAR	CAM	2.5/—	Hurrell et al. (2013)
GISS-E2-H-CC (d)	Goddard Institute for Space Studies (GISS) Model E2, coupled with HYCOM and interactive terrestrial carbon cycle	NASA GISS	GISS LSM	2.5/—	Schmidt et al. (2006)
GISS-E2-H (d)	GISS Model E2, coupled with the HYCOM ocean model	NASA GISS	GISS LSM	2.5/—	Schmidt et al. (2006)
GISS-E2-R-CC (d)	GISS Model E2, coupled with the Russell ocean model and interactive terrestrial carbon cycle	NASA GISS	GISS LSM	2.5/—	Schmidt et al. (2006)
GISS-E2-R (d)	GISS Model E2, coupled with the Russell ocean model	NASA GISS	GISS LSM	2.5/—	Schmidt et al. (2006)
NorESM1-ME (d)	Norwegian ESM (NorESM), version 1 with carbon cycling (and biogeochemistry)	Norwegian Climate Centre	CLM4	2.5/—	Bentsen et al. (2013)
NorESM1-M (d)	NorESM, version 1 (intermediate resolution)	Norwegian Climate Centre	CLM4	2.5/—	Bentsen et al. (2013)
BCC_CSM1.1 (d)	BCC CSM, version 1.1	BCC	BCC_AVIM1.0	2.8125/T42	Wu et al. (2013)
BNU-ESM (w)	Beijing Normal University (BNU)–ESM	BNU	BNU Common Land Model, version 3 (BNU-CoLM3)	2.8125/T42	http://esg.bnu.edu. cn/BNU_ESM_ webs/htmls/index. html
CanESM2 (d)	Second Generation Canadian ESM	Canadian Centre for Climate Modelling and Analysis	Canadian Land Surface Scheme (CLASS)	2.8125/T63	Arora et al. (2011)

TABLE 1. (*Continued*)

Acronym	Expansion	Institution	LSM	Spatial (°)/ spectral resolution	Reference
FGOALS-g2 (d)	Flexible Global Ocean–Atmosphere–Land System Model gridpoint, version 2.0	National Key Laboratory of Numerical Modeling for Atmospheric Sciences and Geophysical Fluid Dynamics (LASG)/ Center for Earth System Science (CESS)	CLM3	2.8125/—	Li et al. (2013)
FIO-ESM (b)	First Institute of Ocean-ography (FIO) ESM	FIO	CLM3.5	2.8125/T42	Qiao et al. (2013)
MIROC-ESM (d)	MIROC ESM	Japan Agency for Marine-Earth Science and Technology (JAMSTEC)	MATSIRO	2.8125/T42	Watanabe et al. (2011)
MIROC-ESM-CHEM (d)	MIROC ESM, Chemistry Coupled	JAMSTEC	MATSIRO	2.8125/T42	Watanabe et al. (2011)
HadCM3 (w)	Hadley Centre Coupled Model, version 3	Met Office Hadley Centre	MOSES	3.75/N48	Johns et al. (2003)

other two reanalysis products. The presence of snow in this area is confirmed by the MODIS satellite snow cover data (Pu et al. 2007). In fact, solid precipitation supplied by southern warm and moist air rising up along the Yarlung Zangbo valley favors a highly persistent snow cover. Over the Tibetan Plateau, BCC_CSM1.1(m), MRI-CGCM3, and CESM1 (BGC) indicate a nonnegligible winter snowpack while the other high-resolution models (EC-EARTH and CMCC-CM) show a very shallow snow depth. Surface observation data available from the Chinese station network confirm the presence of a thick snowpack in winter in the eastern and southeastern portions of the Tibetan Plateau, where average snow depth is locally above 40 cm (Qian et al. 2003).

Most models with a spatial resolution between 1.4° and 2° (ACCESS1.0, CSIRO Mk3.6.0, INM-CM4.0) generally identify a shallower snowpack with respect to the higher-resolution models, with the exception of MIROC5, which is comparable to them. CNRM-CM5 presents an extremely thick snowpack, with unrealistic values up to 30 m (not shown here).

Among the models with an even lower spatial resolution (2.5°–2.8125°), only NorESM1-ME shows a pattern similar to that reproduced by the high-resolution models. The other GCMs either produce a very shallow snowpack over the Himalayan range (CanESM2 and FIO-ESM) or do not properly reproduce the orographic pattern found in the reanalyses (FGOALS-g2 and BCC_CSM1.1). In general, at these resolutions the spatial localization of snow depth over the HKKH range is only coarsely represented.

Another view of these differences is given in Fig. 3, which compares the quantile statistics in the period 1980–2005 of the spatial average over the entire HKKH region (Fig. 1) of the mean DJFMA snow depth, for all

models listed in Table 1. This figure highlights that the models with grid sizes larger than 2.5° tend, with the few exceptions outlined above, to overestimate the snow depth compared to the three reanalysis datasets.

We performed the same analysis for the summer season (JJAS, not shown here). In the reanalyses and in most of the models, the mean JJAS snow depth over the HKKH region is very shallow or even negligible. Many models show the HKK to be snow covered while the Himalayas are represented as mainly snow-free. These results agree with MODIS satellite observations, showing that the Karakoram Range also has a persistent snow cover during summer months. Pu et al. (2007) showed that in the Himalayas the snow cover survives only on the highest-elevation peaks, with the entire Tibetan Plateau retaining approximately 5% snow cover in summer. Despite the fact that the Himalayas receive a considerable amount of precipitation due to the monsoon, this precipitation does not contribute to the creation of a durable and extended snow cover, in part because of the high temperatures that induce fast melting. The GCMs, owing to their coarse resolution, are not able to capture localized summer snow precipitation occurring only at very high elevations; thus, they are not the proper tool to investigate summer variability of snow depth in this area.

2) SNOW WATER EQUIVALENT

To provide an in-depth picture of the available information on snow resources in the HKKH region, we also analyze the snow water equivalent derived from all available datasets. There are 18 GCMs in our CMIP5 ensemble providing SNW at least over the historical period. We exclude CNRM-CM5 from the analyses as it displays extremely high, unrealistic values. Figure 4
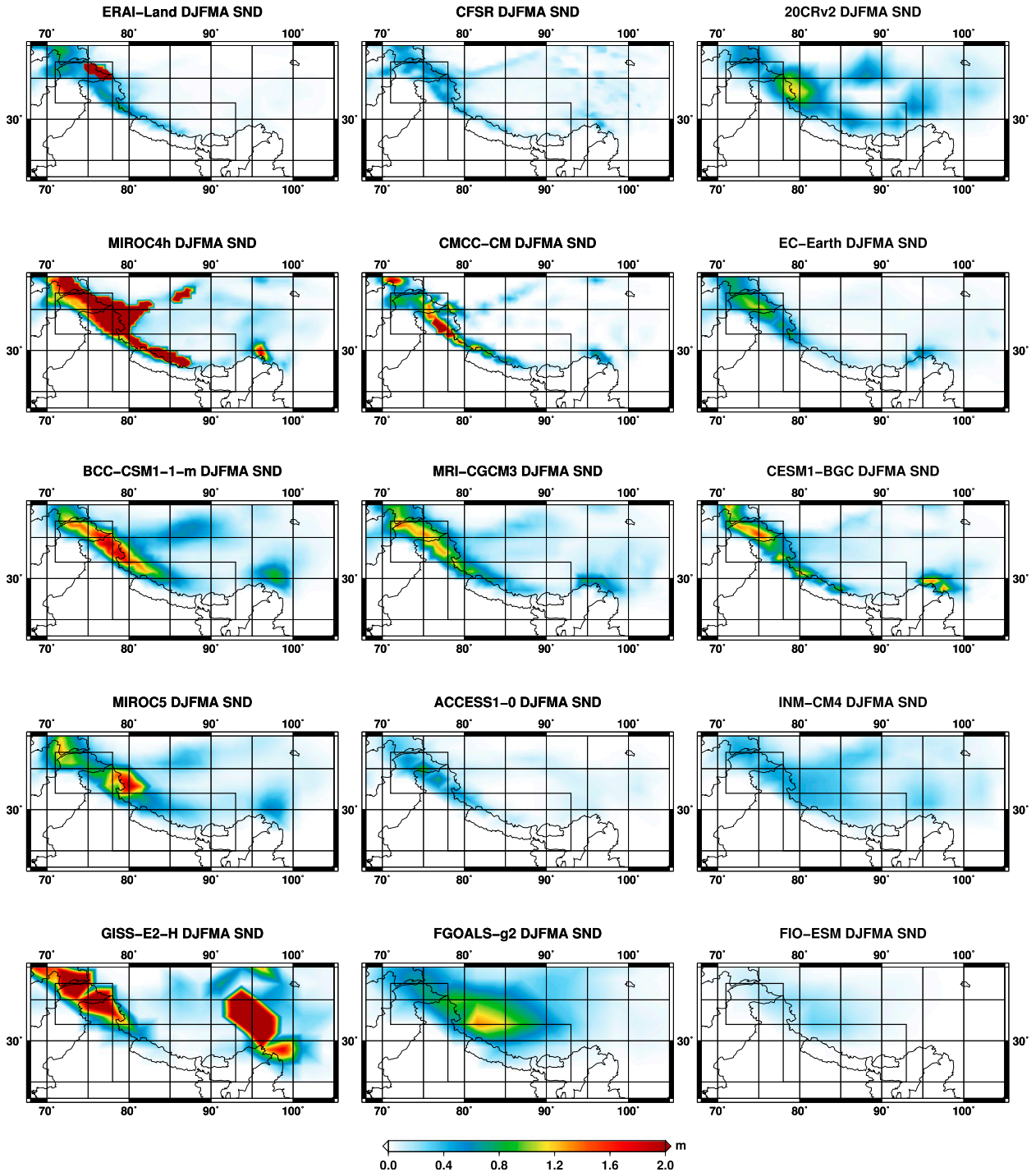
FIG. 2. Spatial distribution of the mean winter (DJFMA) SND for (top row) ERA-Interim/Land, CFSR, 20CRv2, and (other rows) a set of CMIP5 GCMs. The maps represent multiannual means over the period 1980–2005. Reanalyses and models are ordered by decreasing spatial resolution. The boxes highlight the HKK (west) and Himalaya (east) subregions considered in this study.

shows the spatial distribution of the DJFMA SNW averaged over the period 1980–2005. The figure includes also the maps obtained from the AMSR-E/*Aqua* observations and from the CMC snow water equivalent

climatology, even if they refer to shorter and different time periods, 2003–11 and 1998–2011, respectively.

The three reanalyses and the long-term satellite climatology (NSIDC) are in good agreement and
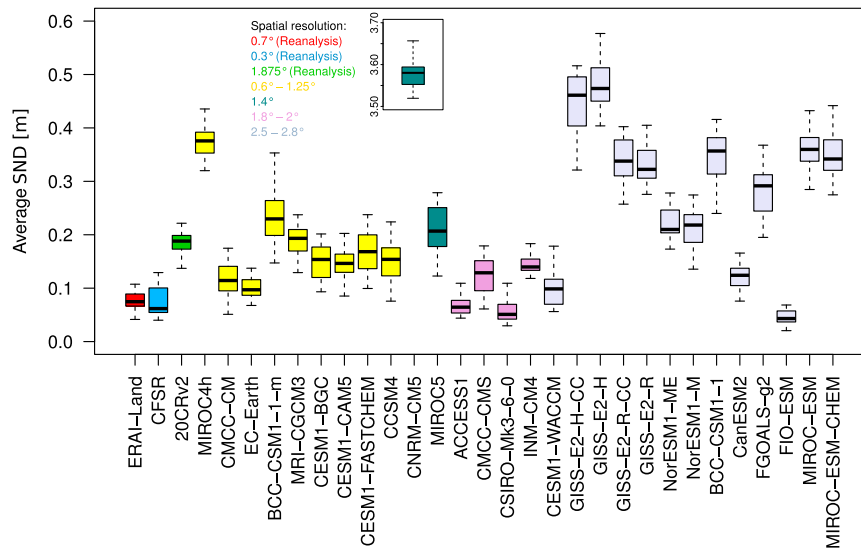
Fig. 3. Spatial average over the HKKH region of mean winter (DJFMA) SND, in the period 1980–2005, for ERA-Interim/Land, CFSR, 20CRv2, and the set of CMIP5 GCMs, ordered by decreasing spatial resolution. Only elevations above 1000 m MSL (excluding the Baltoro area) are considered. The lower hinge, the median, and the upper hinge correspond to the first, second, and third quartiles, respectively, while the lower and upper whiskers represent the min and max values over the period.

represent very similar SNW spatial patterns, coherent with the corresponding snow depth fields. In the last decade, AMSR-E/*Aqua* data present substantially the same spatial pattern of SNW as the longer-term satellite climatology from NSIDC, with slightly higher values with respect to the 1980–2005 mean. In about the same time period spanned by AMSR-E/*Aqua* data, the CMC data present a much thicker snowpack, with peaks up to 2000 kg m^{-2} of snow water equivalent.

The GCMs providing both snow depth and snow water equivalent (see Table 1) show almost the same spatial pattern for the two variables. Similar to what found for snow depth, most GCMs tend to overestimate the SNW with respect to the reanalyses and to the satellite observations, but there is less variability between the different models than for the representation of SND. High- and low-resolution models, in fact, give similar pictures of the SNW spatial pattern. The EC-EARTH and HadGEM2-family models are those that are closest to the reanalyses. CESM1 and CCSM4 show a very similar pattern (indeed, they are based on the same code) and tend to overestimate SNW over the highest-elevation mountains of the HKK and Himalaya regions. Also, the MPI-family models tend to overestimate SNW, mainly for the highest areas of the eastern Karakoram. A more compact view of the intercomparison among all datasets is provided in Fig. 5, showing the quantile statistics in the period 1980–2005 of the spatial average over the entire HKKH region of the mean DJFMA

snow water equivalent. In this case, we do not find a clear separation in the models behavior according to their spatial resolution, as in the analysis of the snow depth shown in Fig. 3.

It is worth noting that the three reanalysis products agree better in their representation of SNW than of SND. In particular, compared to ERA-Interim/Land and CFSR, 20CRv2 presents comparable mean SNW values and higher mean SND values, possibly indicating substantial differences in the estimated snow density in the three products.

b. Historical trends and future projections

We evaluate the past variability of snowpack (SND and SNW) and its expected future changes in the HKKH region, using the reanalyses and all the CMIP5 GCMs. The GCM simulations cover the historical period 1850–2005 and the projection period 2006–2100, under the two Intergovernmental Panel on Climate Change (IPCC) emission scenarios, RCP4.5 and RCP8.5.

For each model, the SND and SNW fields are temporally averaged over the winter season (DJFMA) and spatially averaged over each of the two subdomains, HKK and the Himalayas, weighting each pixel by its fraction of area above 1000 m MSL. Tables 2 and 3 show the DJFMA snow depth mean μ, standard deviation σ, and trend T values for all GCMs providing data at least in the historical period, for the HKK and Himalaya regions, respectively. The significance of the trends is
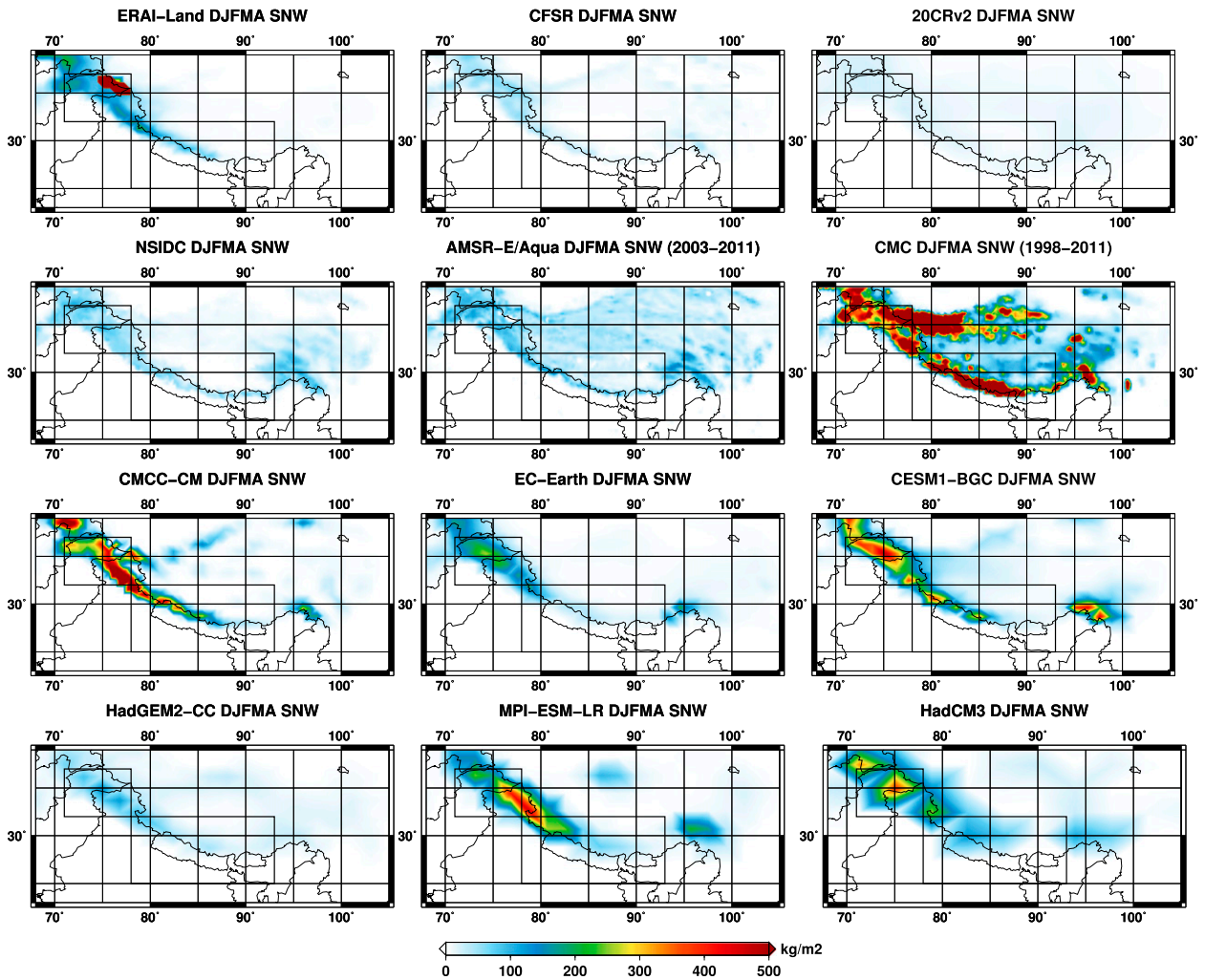
FIG. 4. Spatial distribution of the mean winter (DJFMA) SNW for (top row) ERA-Interim/Land, CFSR, and 20CRv2; (second row) the NSIDC EASE-Grid SNW climatology, the AMSR-E/*Aqua* L3 global SNW, and the CMC SND analysis; and (other rows) a set of CMIP5 GCMs. The maps represent multiannual means over the period 1980–2005, unless otherwise specified. Reanalyses and models are ordered according to decreasing spatial resolution. The boxes highlight the HKK (west) and Himalaya (east) subregions considered in this study.

assessed using a Mann–Kendall test (Sneyers 1990) at significance levels $\alpha = 0.05$ and 0.01.

For a restricted GCM ensemble, including only the high-resolution models, we perform a more detailed investigation aimed at evaluating the extent to which these GCMs are able to represent the time evolution of the snow depth from 1850 to 2100. The high-resolution GCMs taken into account are CMCC-CM, EC-EARTH, BCC_CSM1.1(m), MRI-CGCM3, and CESM1 (BGC), the last one being representative of the four GCMs of the CESM1/CCSM4 family (MIROC4h was not included in this ensemble since its dataset covers only part of the twentieth century). Figure 6 shows the mean winter snow depth time series and the corresponding ensemble mean of the five high-resolution models mentioned above,

compared to the available reanalysis datasets, for both the HKK and the Himalaya domains. The spread between the ensemble members provides a measure the uncertainty of the estimate.

In the HKK subregion, CFSR and 20CRv2 present lower snow depth values in the historical period with respect to the high-resolution GCMs (ERA-Interim/ Land is not included because of its fixed glacier mask over the Baltoro area). The DJFMA long-term-mean snow depth given by 20CRv2 is equal to 37.2 cm over the period 1872–2005, about half of the value provided by the ensemble means of the five high-resolution GCMs (75.4 cm) and of the complete set of models (67.0 cm). The GCM ensemble mean has thus a positive bias with respect to the reanalyses considered here.
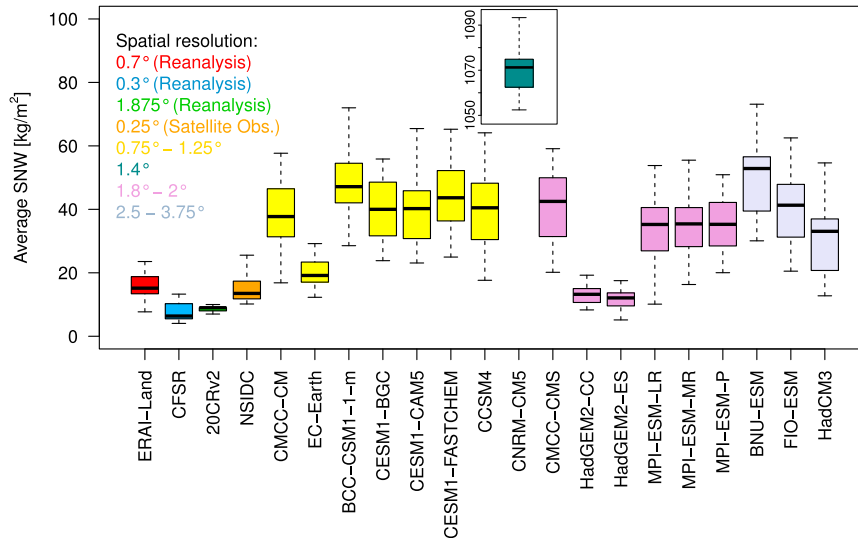
FIG. 5. Spatial average over the HKKH region of mean winter (DJFMA) SNW, in the period 1980–2005, for ERA-Interim/Land, CFSR, 20CRv2, the NSIDC EASE-Grid SNW climatology, and the set of CMIP5 GCMs, ordered by decreasing spatial resolution. Only elevations above 1000 m MSL (excluding the Baltoro area) are considered. The lower hinge, the median, and the upper hinge correspond to the first, second, and third quartiles, respectively, while the lower and upper whiskers represent the min and max values over the period.

In the Himalayas, the GCMs and 20CRv2 are in good agreement, with the reanalysis time series included in the range of variability of the high-resolution model outputs. Comparing the historical mean of area-averaged snow depth, we find similar results for 20CRv2 (23.8 cm), for the ensemble mean over all GCMs (24.8 cm) and for the ensemble mean over high-resolution GCMs only (19.9 cm). ERA-Interim/Land and CFSR present lower snow depth values.

We recall that, since the mean values reported above represent averages over two large boxes that include snow-free areas, they are not representative of the actual average snow height in snow-covered areas.

The ensemble mean over all GCMs indicates, for both scenarios, a significant decreasing trend in the DJFMA snow depth during the historical period, in both domains. The HKK mountains experienced a significant decrease with a trend of $-3.8 \, \text{cm} \, (100 \, \text{yr})^{-1}$, while the Himalayas registered a statistically significant decrease of $-1.9 \, \text{cm} \, (100 \, \text{yr})^{-1}$ [equivalent to a decrease of 5.7% and 7.7% $(100 \, \text{yr})^{-1}$, respectively, compared to the historical mean]. On the other hand, 20CRv2 indicates a statistically significant increasing trend in snow depth in both subregions of the HKKH, at variance with the observed recent regional trends found in the Himalayas and partly in HKK, where several sources indicate retreating glaciers (Kääb et al. 2012; Bolch et al. 2012; Hewitt 2005; Bishop et al. 2008; Hewitt 2011; Gardelle et al. 2012; Sarikaya et al. 2012); this may raise concerns

about the reliability of 20CRv2 for calculating long-term trends in this region.

Future GCM projections indicate that snow depth is expected to significantly decrease in both regions and for both scenarios. The simulations for the HKK in the RCP4.5 scenario indicate a snow depth decrease that is about 3 times stronger than that estimated for the historical period $[-11.6 \, \text{cm} \, (100 \, \text{yr})^{-1}]$; the most extreme RCP8.5 scenario indicates an even stronger, and highly significant, snow depth reduction of $-26.0 \, \text{cm} \, (100 \, \text{yr})^{-1}$ ($\alpha = 0.01$). These rates are equivalent to 17% and 39% $(100 \, \text{yr})^{-1}$ reductions in snow depth compared to the historical mean, respectively. In the Himalayas, the models predict a strong and highly significant ($\alpha = 0.01$) snow depth decrease of -6.2 and $-12.5 \, \text{cm} \, (100 \, \text{yr})^{-1}$ in the RCP4.5 and RCP8.5 scenarios, respectively [equivalent to decreases of 25% and 50% $(100 \, \text{yr})^{-1}$]. The expected relative decrease is much stronger in the Himalayas than in HKK, in agreement with previous studies that found Himalayan glaciers more sensitive to climate change.

Figures 7 and 8 show the spatial patterns of the DJFMA snow depth trends for each of the high-resolution GCMs. The former figure shows the trends in the period 1911–2005, while the latter shows the projection period 2006–2100 under the most extreme RCP8.5 scenario. Both periods span a 95-yr time frame. We report only the trends that are statistically significant at the 95% confidence level (gray areas indicate nonsignificant trends). For the historical period, the GCM

TABLE 2. Winter (DJFMA) SND mean (i.e., μ), std dev (i.e., σ), and trend (i.e., T) for the historical period and for the RCP4.5 and RCP8.5 future scenarios, averaged in the HKK. Trends statistically significant at the 95% (99%) confidence level are indicated with an asterisk (double asterisk). The row ENSEMBLE ALL (in boldface) reports the statistics of the ensemble mean of all models that provide data for both the historical period and for the two RCP projections. The row ENSEMBLE Hi-Res (in boldface) reports the statistics of the ensemble mean of all high-resolution models (in boldface). For comparison, the statistics of 20CRv2 are shown, also in boldface.

Model	Historical			RCP4.5			RCP8.5		
	μ (cm)	σ (cm)	T [cm $(100\,\text{yr})^{-1}$]	μ (cm)	σ (cm)	T [cm $(100\,\text{yr})^{-1}$]	μ (cm)	σ (cm)	T [cm $(100\,\text{yr})^{-1}$]
20CRv2	**37.2**[1]	**9.3**[1]	**4.4***[1]	—	—	—	—	—	—
CMCC-CM	71.2	21.8	−0.1	58.2	20.5	−11.4	50.7	20.9	−34.8**
EC-EARTH	62.9	15.5	−3.9	62.2	18.1	−0.3	55.1	17.4	−18.0**
BCC_CSM1.1(m)	84.3	21.1	−2.3	64.9	17.3	−8.6*	62.0	20.3	−35.5**
MRI-CGCM3	80.1	17.3	−0.5	79.9	19.7	−7.9	78.5	19.5	−3.8
CESM1 (BGC)	78.5	20.7	−7.2*	65.7	22.4	−7.1	59.2	21.7	−30.8**
ENSEMBLE Hi-Res	**75.4**	**8.4**	**−2.8***	**66.2**	**9.5**	**−7.1***	**61.2**	**10.8**	**−24.3****
CCSM4	78.5	19.9	−9.2*	63.2	21.0	−7.3	63.4	22.5	−18.9*
MIROC5	72.6	20.0	−3.9	60.8	21.7	−25.0**	64.5	25.1	−34.5**
ACCESS1.0	41.7	13.4	1.8	32.3	12.9	−14.7*	28.8	12.1	−24.8**
CMCC-CMS	60.8	23.5	−3.7	44.4	18.9	−23.0**	39.1	19.7	−35.9**
CSIRO Mk3.6.0	18.5	9.9	−0.8	18.1	10.2	11.1**	19.6	10.4	3.6
INM-CM4.0	32.0	4.8	−1.7*	27.6	4.6	−0.2	26.9	5.8	−13.7**
GISS-E2-H	176.8	20.6	−22.0**	83.3	21.9	−24.0**	78.9	23.8	−32.4**
GISS-E2-R	163.0	23.4	−17.4**	89.5	18.1	−10.3	87.2	20.4	−35.8**
NorESM1-ME	70.1	16.2	2.9	56.0	16.4	−12.4	51.4	18.6	−38.7**
NorESM1-M	72.1	18.8	−2.8	59.5	17.5	−15.6*	55.0	20.3	−32.9**
BCC_CSM1.1	49.8	14.3	−5.9*	38.7	12.8	−11.4**	30.8	13.1	−24.9**
CanESM2	27.7	11.4	1.1	24.5	9.8	−5.4	24.7	11.7	−9.7
FGOALS-g2	52.3	14.3	−2.1	39.8	13.9	−18.7**	30.8	14.9	−36.7**
FIO-ESM	11.0	4.3	−1.1	7.3	3.0	−2.8*	5.9	3.6	−8.1**
MIROC-ESM-CHEM	53.4	13.6	−2.4	37.1	12.3	−21.5**	27.7	15.5	−43.6**
MIROC-ESM	54.5	14.2	−2.0	35.3	12.8	−27.0**	28.5	15.7	−46.3**
ENSEMBLE ALL	**67.0**	**4.8**	**−3.8****	**49.9**	**4.8**	**−11.6****	**46.8**	**8.0**	**−26.0****
MIROC4h	163.7[2]	16.6[2]	−3.7[2]	146.8[3]	17.4[3]	12.7[3]	—	—	—
CESM1 (CAM5)	62.8	24.6	−0.7	—	—	—	57.5	27.4	−20.8*
CESM1 (FASTCHEM)	81.5	22.8	−8.7	—	—	—	—	—	—
CESM1 (WACCM)	36.0	17.6	−3.7	—	—	—	—	—	—
GISS-E2-H-CC	173.1	27.7	−29.8**	78.5	17.8	−6.9	—	—	—
GISS-E2-R-CC	165.5	25.6	−22.2**	85.5	18.9	5.3	—	—	—

[1] Covers the time period 1872–2005.
[2] Covers the time period 1951–2005.
[3] Covers the time period 2006–35.

results are compared to 20CRv2 (top left). While the reanalysis displays a snow depth increase, especially over the Tibetan Plateau and western Himalayas, the GCMs show more stable snow depth conditions, except for some scattered areas. MRI-CGCM3 identifies a positive trend in the HKK region and CESM1 (BGC) produces a negative trend in the western Himalayas. The 2006–2100 projections in the RCP8.5 scenario (Fig. 8) show a clearer signal in all models with respect to the historical trends (please note the different color scales used in Figs. 7 and 8). The GCMs indicate an overall snow depth decrease everywhere in the HKKH mountain range.

Table 4 reports similar statistics as Tables 2 and 3, but for SNW. Coherently with the SND results, snow water equivalent decreased significantly during the historical period and the registered negative trend, of about 10%

in both Himalayas and HKK, is expected to become stronger in the future decades. The snow water equivalent is projected to decrease by −47% in HKK and by −59% in Himalayas at the end of the twenty-first century in RCP 8.5. Even if intermodel variability of the trend intensity is large, all GCMs agree in projecting a strong and statistically significant decrease of snow resources.

1) AMPLITUDE DISTRIBUTIONS OF SNOW DEPTH

Figure 9 shows the probability distribution function (PDF) of the mean winter snow depth for the high-resolution GCMs, over the HKK and Himalayas and over the period 1980–2005 (in which reanalyses are available). We exclude the Baltoro area from the computation of the PDFs, as ERA-Interim/Land is not reliable there.

TABLE 3. As in Table 2, but for the Himalayas.

	Historical			RCP4.5			RCP8.5		
Model	μ (cm)	σ (cm)	T [cm $(100\,\text{yr})^{-1}$]	μ (cm)	σ (cm)	T [cm $(100\,\text{yr})^{-1}$]	μ (cm)	σ (cm)	T [cm $(100\,\text{yr})^{-1}$]
20CRv2	**23.8**[1]	**7.9**[1]	**4.4***[1]	—	—	—	—	—	—
CMCC-CM	17.2	7.0	0.3	10.8	6.1	−6.3*	9.0	6.7	−16.3**
EC-EARTH	12.4	6.9	−1.9*	8.2	5.1	−5.0*	6.9	4.7	−7.6**
BCC_CSM1.1(m)	25.3	10.8	−0.1	19.8	9.3	−13.8**	17.6	9.4	−16.2**
MRI-CGCM3	23.2	7.1	−2.0	19.0	6.2	−5.1	17.2	6.6	−7.1**
CESM1 (BGC)	21.5	9.1	−2.3	16.6	8.2	−1.4	13.3	7.7	−9.2**
ENSEMBLE Hi-Res	**19.9**	**3.9**	**−1.2**	**14.9**	**3.6**	**−6.3****	**12.9**	**4.2**	**−11.1****
CCSM4	22.1	10.3	−3.5	16.4	8.7	−0.9	13.3	6.9	−6.1*
MIROC5	26.8	9.3	−1.8	18.6	8.4	−12.2**	18.8	10.2	−18.2**
ACCESS1.0	7.4	3.4	−1.1	3.4	2.3	−3.9**	2.9	2.2	−5.0**
CMCC-CMS	22.0	10.0	−1.7	13.0	7.7	−9.8**	9.7	6.2	−14.0**
CSIRO Mk3.6.0	7.6	4.3	−1.4*	4.9	2.9	3.1**	5.3	2.9	−2.2
INM-CM4.0	20.1	5.3	−2.5*	16.3	5.8	−1.6	14.2	5.7	−9.8**
GISS-E2-H	11.8	4.4	−2.2**	10.0	3.7	−3.6**	8.8	3.6	−3.6*
GISS-E2-R	7.7	2.5	0.9	7.7	3.1	−1.7	6.8	3.0	−4.6**
NorESM1-ME	37.7	11.4	−1.9	30.8	10.7	−6.8*	27.9	10.6	−13.9**
NorESM1-M	38.1	12.9	−1.2	32.0	10.2	−3.5	29.0	10.8	−14.5**
BCC_CSM1.1	55.4	15.4	−5.6	45.4	10.9	−5.8	41.1	12.3	−22.0**
CanESM2	13.9	6.1	0.3	11.1	5.4	−2.9	10.7	5.7	−5.5*
FGOALS-g2	38.5	10.4	0.6	30.4	9.1	−11.6**	28.3	9.3	−16.5**
FIO-ESM	5.9	2.4	−0.7	5.2	2.0	0.4	4.4	1.8	−0.5
MIROC-ESM-CHEM	59.0	14.7	−7.4**	42.8	12.2	−20.9**	33.3	13.6	−38.9**
MIROC-ESM	60.6	13.9	−5.3	40.5	11.6	−16.0**	34.0	15.0	−41.4**
ENSEMBLE ALL	**24.8**	**2.0**	**−1.9****	**19.2**	**2.4**	**−6.2****	**16.5**	**3.7**	**−12.5****
MIROC4h	49.1[2]	7.6[2]	−10.4[2]	30.4[3]	8.0[3]	−40.7*[3]	—	—	—
CESM1 (CAM5)	11.1	6.3	−0.5	—	—	—	8.6	5.4	−3.7
CESM1 (FASTCHEM)	22.6	9.4	0.4	—	—	—	—	—	—
CESM1 (WACCM)	7.5	5.6	−1.3	—	—	—	—	—	—
GISS-E2-H-CC	11.4	3.6	−0.3	9.6	3.5	−2.1	—	—	—
GISS-E2-R-CC	8.0	2.8	0.3	6.8	2.8	−0.2	—	—	—

[1] Covers the time period 1872–2005.
[2] Covers the time period 1951–2005.
[3] Covers the time period 2006–35.

In the HKK region, the PDF of 20CRv2 is very close to the CFSR for low SND values (up to about 0.8 m) and is very close to the distribution of ERA-Interim/Land at higher values. In the Himalayas, ERA-Interim/Land and 20CRv2 PDFs present similar upper tails. In both subregions, CFSR presents lower high tails compared to both ERA-Interim/Land and 20CRv2.

The PDFs of the GCMs have generally higher tails compared to the reanalyses, that is, they display more extreme snow depth values. The EC-EARTH model produces the SND distribution that is closest to the reanalyses (in the Himalayas, they are almost coincident with ERA-Interim/Land), probably owing to the fact that this model and ERA-Interim share the same atmospheric module and a similar land surface scheme. MIROC4h has a rather flat PDF with respect to all other GCMs in both subregions, meaning more frequent high snow depth values, as we have already seen in the analysis of the SND spatial distribution. In general,

the analysis of the PDFs supports the finding that the agreement between models and reanalyses is higher in the Himalayas compared to the HKK.

2) SEASONAL CYCLE OF SNOW DEPTH

Figure 10 (top) shows the annual cycle of snow depth averaged over the high-elevation pixels (>1000 m MSL) of the HKK and Himalayas, as represented by the high-resolution GCMs and by the three reanalysis datasets. Also in this case the temporal averages refer to the period 1980–2005.

In both the HKK and the Himalayas, the models and the reanalyses display a unimodal snow regime, with the snow depth maximum generally occurring in February–March. It is interesting to note that CFSR and 20CRv2 identify the snow depth peak in February, while in ERA-Interim/Land the accumulation phase dominates also in March. Afterward, snow depth decreases to almost complete melting in July/August. In HKK, the

DJFMA snow depth projections − HKK above 1000 m a.s.l.

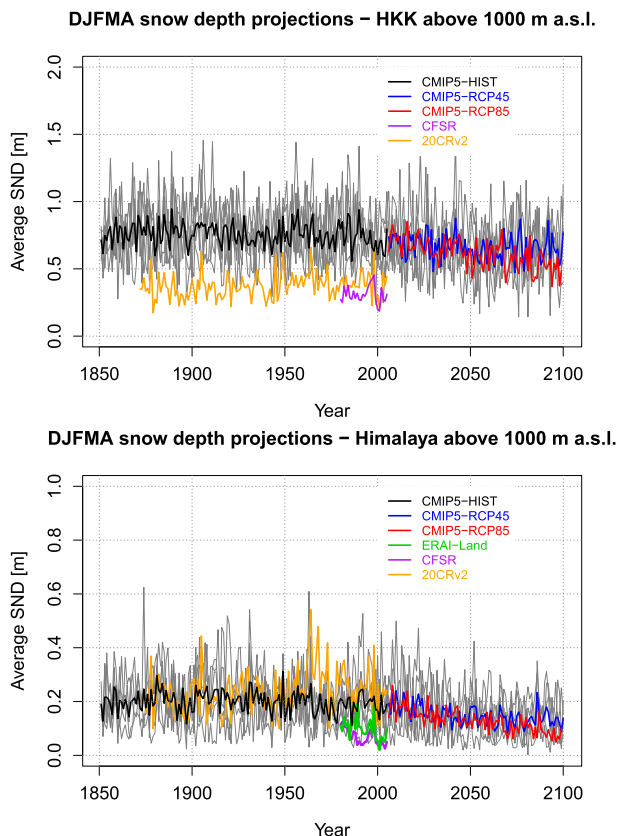**DJFMA snow depth projections − Himalaya above 1000 m a.s.l.**

FIG. 6. Time series of mean winter (DJFMA) SND in the historical period and for the twenty-first century (RCP4.5 and RCP8.5 scenarios), averaged over the (top) HKK and (bottom) Himalayas. Gray lines represent the high-resolution CMIP5 models. Boldface lines represent the ensemble means of historical (black), RCP4.5 (blue), and RCP8.5 (red) simulations. The other colored lines represent the reanalysis data. Only elevations above 1000 m MSL are considered in the spatial average. Please note that ERA-Interim/Land is not shown in the HKK plot, as its SND is not reliable in the Baltoro area.

snowpack is deeper than in the Himalayas (please note the different vertical scale).

In the HKK subregion, the multimodel ensemble mean overestimates the snow depth values compared to the reanalyses, while in the Himalayas it lies inside the range of variability of the reanalyses. Note though that while in HKK the spread among the GCMs is relatively small and the three reanalyses agree well with each other, in the Himalayas, the GCM spread is large, as is the difference among the reanalyses (the 20CRv2 data, in fact, present significantly higher values compared to the ERA-Interim/Land and CFSR data). This indicates high uncertainty in the estimation of the snowpack thickness in the Himalayas.

Figure 10 (bottom) shows the temporal variability of the ensemble mean of the seasonal cycles in the historical period, reporting the snow regimes during the three

subperiods 1851–1900, 1901–50, and 1951–2000. Very similar features are found in the first two subperiods, while in 1951–2000, the models show a decrease in the March–April (Himalayas) and April–May (HKK) snow depth, and thus an earlier spring snowmelt.

Looking at the twenty-first-century projections (also in Fig. 10, bottom), a considerable snow depth decrease in the HKK and the Himalayas is found, for both the RCP4.5 and RCP8.5 scenarios. In particular, the seasonal snow depth peak in the Himalayas is expected to shift from March to February, resulting in a change in the timing of melting and of water discharge. In the nearest future (2001–50), the models indicate relatively small differences between the RCP4.5 and RCP8.5 scenarios while the projections diverge in the second half of the century, when the snowpack is projected to be more sensitive to the external forcings.

4. Summary and conclusions

We investigated how the snowpack of a crucial but poorly instrumented mountain region, the HKKH, is represented in the main available observational datasets, three reanalysis products, and the state-of-the-art CMIP5 GCMs, by considering the snow depth and snow water equivalent variables. We analyzed and compared the spatial and temporal distribution of snowpack, its annual cycle, and its time evolution in the historical period, using all available datasets, and discussed the CMIP5 model projections under two future climate change scenarios.

The models with higher spatial resolution (0.56°–1.25°) provide a representation of the snow depth distribution that is consistent with ERA-Interim/Land, CFSR, and 20CRv2 data. Several lower-spatial-resolution models tend to represent either a very thick or very shallow snowpack in winter or even show a snow cover pattern that is not consistent with the orographic features. The higher-resolution models are in fair agreement with each other and with the reanalyses in terms of spatial pattern of snow cover and mean thickness of snowpack spatially averaged over the whole HKKH area. However, focusing on the two subdomains separately, HKK and the Himalayas, we find different behaviors. In the HKK, the uncertainty in the estimate of the snowpack thickness by the reanalyses is relatively small, as is the spread among the GCMs. The GCMs ensemble mean clearly overestimates snow depth compared to the reanalyses. In the Himalayas, both the uncertainties in the reanalyses and the spread among GCMs are larger, with the GCMs' ensemble mean lying inside the range of variability of the reanalyses. In conclusion, in terms of snow depth, the GCM ensemble mean compares well with the reanalyses
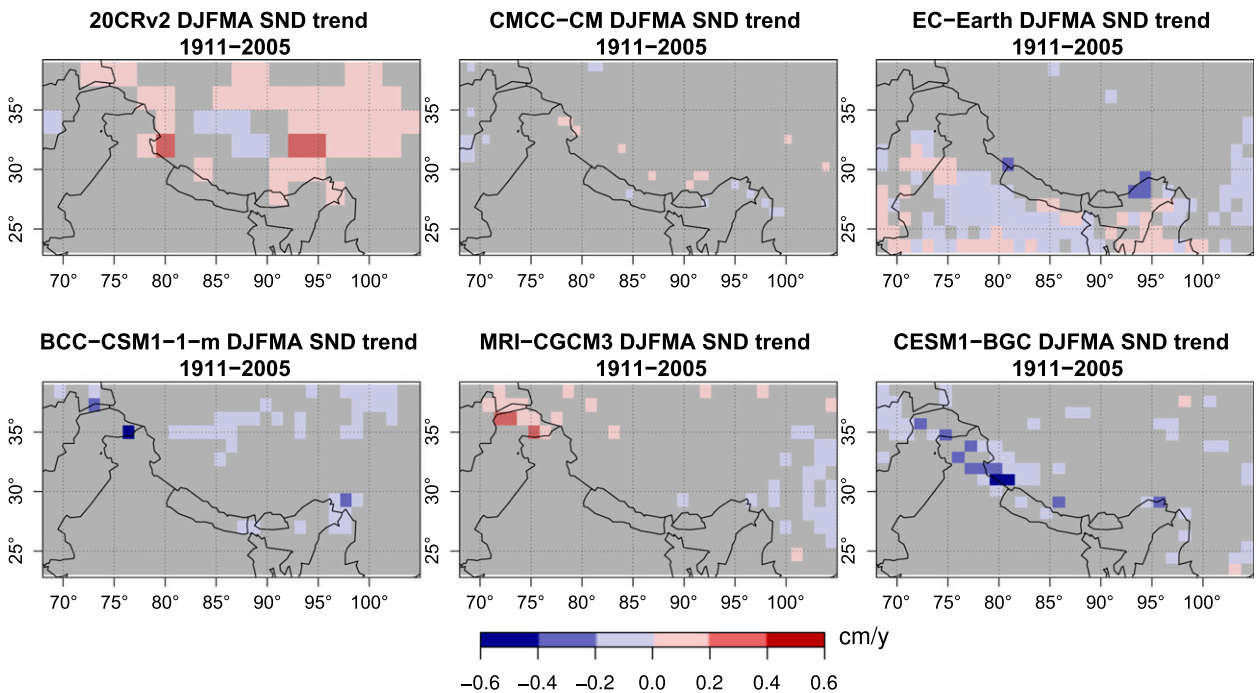
FIG. 7. Spatial distribution of the winter (DJFMA) trends of SND, estimated over the period 1911–2005 and significant at the 95% confidence level.

(in the Himalayas) or provides an overestimation (in the HKK); however, a correct interpretation of these results requires some caution, since in the HKKH, the reanalyses assimilate very few surface observations, do not assimilate snow depth, and may be affected by higher uncertainties than in other regions having better instrumental coverage. The lower agreement between coarse-resolution models and the reanalyses is presumably due to the fact that they run at very different resolutions. Additionally, the coarse GCM resolution smooths out topography too much and may allow precipitation to migrate farther into the Tibetan Plateau.
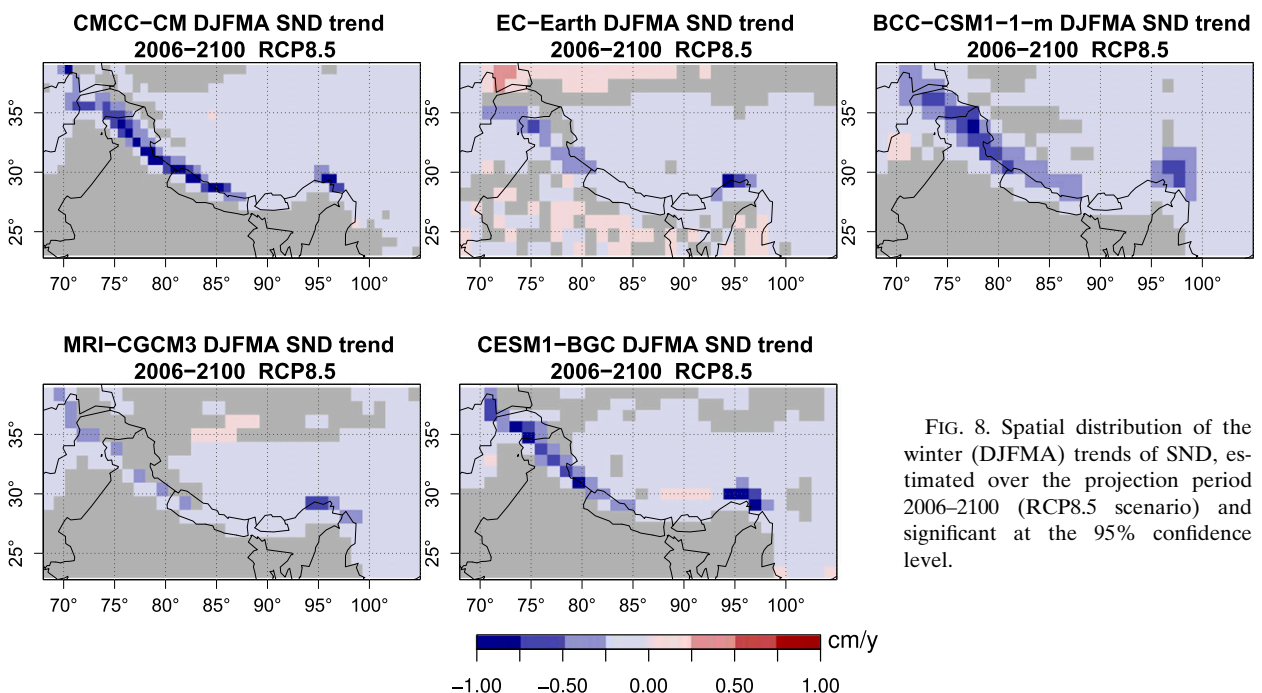

FIG. 8. Spatial distribution of the winter (DJFMA) trends of SND, estimated over the projection period 2006–2100 (RCP8.5 scenario) and significant at the 95% confidence level.

TABLE 4. Winter (DJFMA) SNW mean (i.e., μ), std dev (i.e., σ), and trend (i.e., T) for the historical period and for the RCP4.5 and RCP8.5 future scenarios, averaged in the HKK and Himalaya regions. Trends statistically significant at 95% (99%) confidence level are indicated with an asterisk (double asterisk). The row ENSEMBLE (in boldface) reports the statistics of the ensemble mean of all models that provide data for both the historical period and for the two RCP projections.

Model	Historical			RCP4.5			RCP8.5		
	μ (kg m^{-2})	σ (kg m^{-2})	T [kg m^{-2} (100 yr)$^{-1}$]	μ (kg m^{-2})	σ (kg m^{-2})	T [kg m^{-2} (100 yr)$^{-1}$]	μ (kg m^{-2})	σ (kg m^{-2})	T [kg m^{-2} (100 yr)$^{-1}$]
HKK									
CMCC-CM	235.2	72.0	−0.2	192.0	67.5	−37.6	167.3	69.1	−115.0**
EC-EARTH	136.3	40.2	−9.3	140.0	47.4	7.8	122.7	45.5	−37.0*
CESM1 (BGC)	230.5	69.9	−20.3	192.2	75.9	−19.0	172.3	70.7	−92.6***
CCSM4	232.6	68.7	−28.4*	185.3	70.0	−22.6	189.3	75.9	−54.7
CMCC-CMS	200.5	77.4	−12.0	146.4	62.5	−76.0**	129.1	65.2	−118.4**
HadGEM2-CC	62.2[1]	23.6[1]	0.0[1]	45.7	20.7	−19.9**	39.3	25.5	−48.5**
HadGEM2-ES	66.0[1]	27.6[1]	5.5[1]	47.8	27.8	−33.8**	37.7	21.5	−33.9**
MPI-ESM-LR	160.9	58.5	−20.3*	156.3	63.0	−29.4	118.6	66.6	−119.8**
MPI-ESM-MR	184.3	64.26	−8.8	156.4	63.0	−29.8	162.7	71.7	−91.1**
ENSEMBLE	**169.3**	**19.9**	**−16.7****	**140.2**	**23.2**	**−28.9****	**126.5**	**28.4**	**−79.0****
BCC_CSM1.1(m)	207.7	53.3	−13.2	—	—	—	—	—	—
CESM1 (CAM5)	172.4	87.6	15.8	—	—	—	—	—	—
CESM1 (FASTCHEM)	240.8	75.8	−26.6	—	—	—	—	—	—
MPI-ESM-P	178.9	67.3	−12.8	—	—	—	—	—	—
BNU-ESM	92.0	41.5	−6.5	—	—	—	—	—	—
FIO-ESM	129.1	44.8	−10.4	—	—	—	—	—	—
HadCM3	200.8[1]	84.6[1]	27.0[1]	229.0[2]	67.9[2]	−144.6[2]	—	—	—
Himalayas									
CMCC-CM	56.9	23.1	1.1	35.5	20.2	−21.0*	29.6	22.2	−16.4**
EC-EARTH	25.0	16.0	−3.8	15.9	11.5	−11.0*	13.4	11.2	−16.4**
CESM1 (BGC)	59.0	28.6	−5.5	44.3	25.0	−2.6	34.4	23.3	−24.2***
CCSM4	61.1	33.8	−10.8	44.7	27.2	−0.7	35.8	21.5	−15.6
CMCC-CMS	72.7	33.1	−5.7	42.8	25.4	−32.0**	32.0	20.5	−46.0**
HadGEM2-CC	16.5[1]	7.4[1]	2.6[1]	11.6	6.1	−7.1**	9.6	7.0	−14.7**
HadGEM2-ES	13.3[1]	6.9[1]	1.5[1]	8.4	6.2	−10.5**	7.4	6.1	−10.4**
MPI-ESM-LR	52.0	27.9	−3.0	41.0	21.0	−10.4	28.3	20.7	−33.3***
MPI-ESM-MR	57.2	28.2	−6.1	41.0	21.0	−10.4	35.3	21.8	−33.5***
ENSEMBLE	**46.5**	**8.3**	**−5.2****	**31.7**	**8.1**	**−11.7****	**25.1**	**9.6**	**−27.6****
BCC_CSM1.1(m)	54.0	26.4	1.4	—	—	—	—	—	—
CESM1 (CAM5)	29.7	18.9	2.6	—	—	—	—	—	—
CESM1 (FASTCHEM)	62.6	29.1	1.9	—	—	—	—	—	—
MPI-ESM-P	51.8	26.5	−9.5	—	—	—	—	—	—
BNU-ESM	72.2	28.7	3.4	—	—	—	—	—	—
FIO-ESM	75.6	30.3	−7.1	—	—	—	—	—	—
HadCM3	44.6[1]	24.3[1]	6.8[1]	47.6[2]	25.5[2]	−99.9[2]	—	—	—

[1] Covers the time period 1860–2005.
[2] Covers the time period 2006–2035.

PDF of DJFMA snow depth

HKK above 1000 m a.s.l.

PDF of DJFMA snow depth
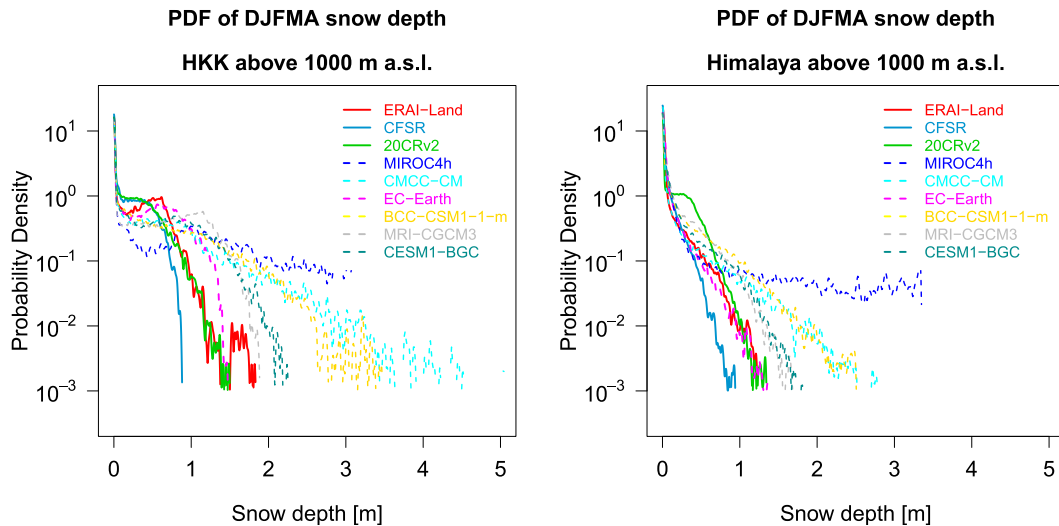
Himalaya above 1000 m a.s.l.

FIG. 9. PDFs of mean winter (DJFMA) SND, computed over the period 1980–2005 and for all grid points in the (left) HKK (excluding the Baltoro area) and (right) Himalayas for the CMIP5 models and the reanalyses.

The distribution and the average values of snow water equivalent are reproduced in a similar way in all reanalyses. Fewer GCMs provide this variable compared to snow depth. While providing a rather consistent representation, most GCMs tend to overestimate SNW compared to reanalyses, except for EC-EARTH and HadGEM2.

The analysis of the mean DJFMA snow depth and snow water equivalent in the historical period (1850–2005) indicates a significant decrease in snow resources in the HKK and Himalayas, which is expected to continue in future decades. Future projections (2006–2100) show a significant, and stronger, winter snow depth decrease in both regions. The HKK is expected to undergo a snow depth decrease of about 17% with respect to the historical mean value in the RCP4.5 scenario and of about 39% in the RCP8.5 scenario. The Himalayas will face a significantly stronger decrease, ranging from 25% up to 50% of current conditions in the most extreme RCP8.5 scenario.

The GCM results indicate that, in the period 1951–2000, the mean spring snow depth decreased with respect to previous 50-yr periods (1851–1900 and 1901–50). In the HKK, this decrease occurred mainly from April to May, while in the Himalayas it started even earlier, in March. Future projections indicate a general decrease of snow depth throughout the snow season, from October to June, which is strongest in the RCP8.5 scenario. In the Himalaya region, the models project a shift in the snow depth maximum from March to February, resulting in an earlier spring snowmelt and a consequent shift in the timing of water discharge. It has to be remarked that these results refer to quite coarse

model resolutions. So, while the net balance may be decreasing over the entire region, current field data and several glacier mass balances show that SND and SNW in the HKK are increasing at some high-elevation locations, but decreasing at lower elevations (Hewitt 2005; Bishop et al. 2008; Hewitt 2011; Gardelle et al. 2012; Sarikaya et al. 2012). Resolving this behavior would require much higher resolutions than those of the current CMIP5 models.

Our results on HKKH snow depth and snow water equivalent can be interpreted in a wider perspective considering the temperature and precipitation changes that occurred in this region. Su et al. (2013) showed that most CMIP5 GCMs tend to underestimate the observed temperature, especially in winter, and that the multimodel ensemble mean has a cold bias of 1.2°–2.5°C in the DJFMA period. On the contrary, precipitation is overestimated over the Tibetan Plateau and has a strong positive bias with respect to observations. The combination of colder surface temperatures and wetter conditions may explain the GCMs overestimation of snow thickness identified here, particularly in the HKK region.

Over the Tibetan Plateau (Su et al. 2013), the GCMs predict steadily increasing annual temperatures in the twenty-first century under the RCP8.5 scenario; the winter season is projected to warm the most, while the summer season the least. The long-term mean temperature increase, relative to the mean over 1961–2005, is 4.1°C for the RCP8.5 scenario (Su et al. 2013).

Historical and future precipitation trends in the HKKH region are much more uncertain than temperature trends, as indicated by the large discrepancies among the models. A recent study by Palazzi et al. (2014,
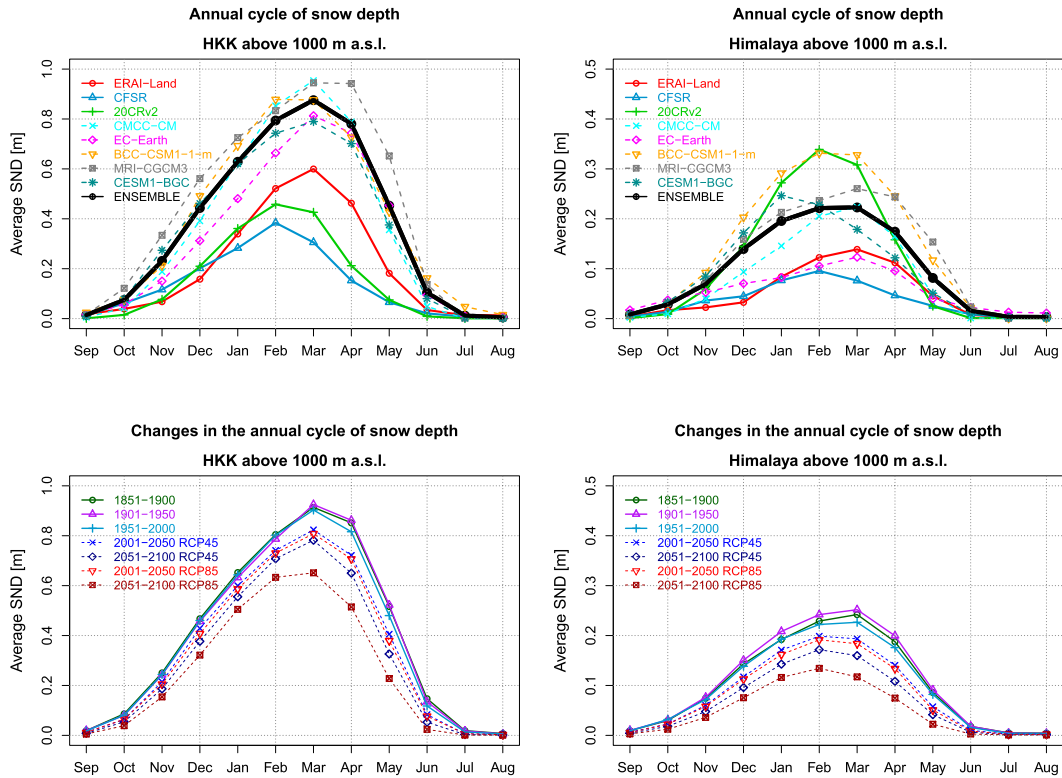
FIG. 10. Seasonal cycle of average SND in (left) HKK (excluding the Baltoro area in the top left) and (right) Himalayas above 1000 m MSL, obtained from the high-resolution CMIP5 GCMs. (top) Multiannual monthly means over the period 1980–2005 compared to reanalyses; (bottom) means over time slices of 50 years in the historical period and in the projection period under the RCP4.5 and RCP8.5 scenarios.

manuscript submitted to *Climate Dyn.*) shows that in the HKK region in winter, the GCM ensemble mean indicates significant negative precipitation trends during the historical period and for the future decades. In the Himalayas, the CMIP5 GCM ensemble mean does not indicate significant winter precipitation trends, in both the historical period and in future decades, with about half of the models providing negative trends of precipitation and the other half providing positive, increasing precipitation trends.

These considerations suggest that the decreasing snow depth trends in the HKK and Himalayas, both in the historical period and in the twenty-first-century projections, are mainly driven by the increase in winter temperatures, at least in the Himalayan range. In the HKK, warmer temperatures and drier winters are expected to interplay to give rise to a considerably less thick and durable snowpack, especially in the second half of the twenty-first century.

Overall, the CMIP5 ensemble provides important information on the HKKH snow climatology and its expected changes in a warming climate, despite the fact that the view provided by the GCMs is spatially smoothed, owing to their coarse spatial resolution compared to the rapidly varying topography of this area. Absolute validation of GCM results against "ground truth" remains a challenge in such orographically complex areas, because of the insufficient availability of surface observations. Nevertheless, the comparison of model outputs with currently available reanalyses and satellite products provides important information on the capability of CMIP5 GCMs to reproduce climate patterns even in these poorly instrumented areas. The results discussed in this study, identifying the uncertainties in the state-of-the-art CMIP5 GCM simulations, should be taken into account when using snow-related GCM outputs for hydrological modeling or climate impact studies in the HKKH.

REFERENCES

Archer, D. R., and H. Fowler, 2004: Spatial and temporal variations in precipitation in the upper Indus basin, global teleconnections and hydrological implications. *Hydrol. Earth Syst. Sci.,* **8,** 47–61, doi:10.5194/hess-8-47-2004.

Armstrong, R., M. Brodzik, K. Knowles, and M. Savoie, 2005: Global monthly EASE-Grid snow water equivalent climatology [1979–2005]. National Snow and Ice Data Center, Boulder, CO, digital media. [Available online at http://nsidc.org/data/nsidc-0271.]

Arora, V., and Coauthors, 2011: Carbon emission limits required to satisfy future representative concentration pathways of greenhouse gases. *Geophys. Res. Lett.,* **38,** L05805, doi:10.1029/2010GL046270.

Balsamo, G., A. Beljaars, K. Scipal, P. Viterbo, B. van den Hurk, M. Hirschi, and A. K. Betts, 2009: A revised hydrology for the ECMWF model: Verification from field site to terrestrial water storage and impact in the integrated forecast system. *J. Hydrometeor.,* **10,** 623–643, doi:10.1175/2008JHM1068.1.

——, and Coauthors, 2012: ERA-Interim/Land: A global land-surface reanalysis based on ERA-Interim meteorological forcing. ERA Rep. Series 13, ECMWF, 25 pp.

——, and Coauthors, 2013: ERA-Interim/Land: A global land water resources dataset. *Hydrol. Earth Syst. Sci. Discuss.,* **10,** 14 705–14 745, doi:10.5194/hessd-10-14705-2013.

Bao, X., and F. Zhang, 2013: Evaluation of NCEP–CFSR, NCEP–NCAR, ERA-Interim, and ERA-40 reanalysis datasets against independent sounding observations over the Tibetan Plateau. *J. Climate,* **26,** 206–214, doi:10.1175/JCLI-D-12-00056.1.

Bentsen, M., and Coauthors, 2013: The Norwegian Earth System Model, NorESM1-M—Part 1: Description and basic evaluation of the physical climate. *Geosci. Model Dev.,* **6,** 687–720, doi:10.5194/gmd-6-687-2013.

Bi, D., and Coauthors, 2013: The ACCESS coupled model: Description, control climate and evaluation. *Aust. Meteor. Oceanogr. J.,* **63,** 9–32.

Bishop, M., A. Bush, E. Collier, L. Copland, U. Haritashya, S. John, S. Swenson, and J. Wahr, 2008: Advancing glaciers and positive mass anomaly in the Karakoram Himalaya, Pakistan. *Eos, Trans. Amer. Geophys. Union,* **89** (Fall Meeting Suppl.), Abstract C32B-04.

Bolch, T., and Coauthors, 2012: The state and fate of Himalayan glaciers. *Science,* **336,** 310–314, doi:10.1126/science.1215828.

Bookhagen, B., and D. Burbank, 2010: Toward a complete Himalayan hydrological budget: Spatiotemporal distribution of snowmelt and rainfall and their impact on river discharge. *J. Geophys. Res.,* **115,** F03019, doi:10.1029/2009JF001426.

Brown, R., and B. Brasnett, 2010: Canadian Meteorological Centre (CMC) daily snow depth analysis data [1998–2011]. National Snow and Ice Data Center, Boulder, CO, digital media. [Available online at http://nsidc.org/data/nsidc-0447.]

Brutel-Vuilmet, C., M. Menegoz, and G. Krinner, 2013: An analysis of present and future seasonal Northern Hemisphere land snow cover simulated by CMIP5 coupled climate models. *Cryosphere,* **7,** 67–80, doi:10.5194/tc-7-67-2013.

Collier, M., and Coauthors, 2011: The CSIRO-Mk3.6.0 Atmosphere–Ocean GCM: Participation in CMIP5 and data publication. *Proc. 19th Int. Congress on Modelling and Simulation,* Perth, Australia, MSSANZ, 2691–2697. [Available online at www.mssanz.org.au/modsim2011/F5/collier.pdf.]

Collins, W., and Coauthors, 2011: Development and evaluation of an Earth-system model–HadGEM2. *Geosci. Model Dev.,* **4,** 1051–1075, doi:10.5194/gmd-4-1051-2011.

Compo, G. P., and Coauthors, 2011: The Twentieth Century Reanalysis Project. *Quart. J. Roy. Meteor. Soc.,* **137,** 1–28, doi:10.1002/qj.776.

Dahe, Q., L. Shiyin, and L. Peiji, 2006: Snow cover distribution, variability, and response to climate change in western China. *J. Climate,* **19,** 1820–1833, doi:10.1175/JCLI3694.1.

Dee, D. P., and Coauthors, 2011: The ERA-Interim reanalysis: Configuration and performance of the data assimilation system. *Quart. J. Roy. Meteor. Soc.,* **137,** 553–597, doi:10.1002/qj.828.

Dutra, E., G. Balsamo, P. Viterbo, P. M. Miranda, A. Beljaars, C. Schär, and K. Elder, 2010: An improved snow scheme for the ECMWF land surface model: Description and offline validation. *J. Hydrometeor.,* **11,** 899–916, doi:10.1175/2010JHM1249.1.

Gardelle, J., E. Berthier, and Y. Arnaud, 2012: Slight mass gain of Karakoram glaciers in the early twenty-first century. *Nat. Geosci.,* **5,** 322–325, doi:10.1038/ngeo1450.

Gent, P. R., and Coauthors, 2011: The Community Climate System Model version 4. *J. Climate,* **24,** 4973–4991, doi:10.1175/2011JCLI4083.1.

Giorgetta, M. A., and Coauthors, 2013: Climate and carbon cycle changes from 1850 to 2100 in MPI-ESM simulations for the Coupled Model Intercomparison Project phase 5. *J. Adv. Model. Earth Syst.,* **5,** 572–597, doi:10.1002/jame.20038.

Hastings, D., and P. Dunbar, 1999: Global Land One-kilometer Base Elevation (GLOBE) digital elevation model documentation, volume 1.0. Key to Geophysical Records Doc. 34, NOAA/NESDIS/NGDC, Boulder, CO, 139 pp. [Available online at www.ngdc.noaa.gov/mgg/topo/report/globedocumentationmanual.pdf.]

Hazeleger, W., and Coauthors, 2012: EC-Earth V2.2: Description and validation of a new seamless Earth system prediction model. *Climate Dyn.,* **39,** 2611–2629, doi:10.1007/s00382-011-1228-5.

Hewitt, K., 2005: The Karakoram anomaly? Glacier expansion and the 'Elevation Effect,' Karakoram Himalaya. *Mt. Res. Dev.,* **25,** 332–340, doi:10.1659/0276-4741(2005)025[0332:TKAGEA]2.0.CO;2.

——, 2011: Glacier change, concentration, and elevation effects in the Karakoram Himalaya, upper Indus basin. *Mt. Res. Dev.,* **31,** 188–200, doi:10.1659/MRD-JOURNAL-D-11-00020.1.

Hurrell, J. W., and Coauthors, 2013: The Community Earth System Model: A framework for collaborative research. *Bull. Amer. Meteor. Soc.,* **94,** 1339–1360, doi:10.1175/BAMS-D-12-00121.1.

Johns, T., and Coauthors, 2003: Anthropogenic climate change for 1860 to 2100 simulated with the HadCM3 model under updated emissions scenarios. *Climate Dyn.,* **20,** 583–612, doi:10.1007/s00382-002-0296-y.

Kääb, A., E. Berthier, C. Nuth, J. Gardelle, and Y. Arnaud, 2012: Contrasting patterns of early twenty-first-century glacier mass change in the Himalayas. *Nature,* **488,** 495–498, doi:10.1038/nature11324.

Li, L., and Coauthors, 2013: The Flexible Global Ocean–Atmosphere–Land System Model, Grid-point version 2: FGOALS-g2. *Adv. Atmos. Sci.,* **30,** 543–560, doi:10.1007/s00376-012-2140-6.

Liniger, H., R. Weingartner, and M. Grosjean, 1998: Mountains of the world: Water towers for the 21st century. Tech. Rep., Centre for Development and Environment, University of Bern, Bern, Switzerland, 32 pp.

Ma, L., T. Zhang, O. Frauenfeld, B. Ye, D. Yang, and D. Qin, 2009: Evaluation of precipitation from the ERA-40, NCEP-1, and NCEP-2 reanalyses and CMAP-1, CMAP-2, and GPCP-2 with ground-based measurements in China. *J. Geophys. Res.,* **114,** D09105, doi:10.1029/2008JD011178.

Moss, R. H., and Coauthors, 2010: The next generation of scenarios for climate change research and assessment. *Nature,* **463,** 747–756, doi:10.1038/nature08823.

Palazzi, E., J. von Hardenberg, and A. Provenzale, 2013: Precipitation in the Hindu-Kush Karakoram Himalaya: Observations and future scenarios. *J. Geophys. Res. Atmos.,* **118,** 85–100, doi:10.1029/2012JD018697.

Pu, Z., L. Xu, and V. V. Salomonson, 2007: MODIS/Terra observed seasonal variations of snow cover over the Tibetan Plateau. *Geophys. Res. Lett.,* **34,** L06706, doi:10.1029/2007gl029262.

Putkonen, J. K., 2004: Continuous snow and rain data at 500 to 4400 m altitude near Annapurna, Nepal, 1999–2001. *Arct. Antarct. Alp. Res.,* **36,** 244–248, doi:10.1657/1523-0430(2004)036[0244:CSARDA]2.0.CO;2.

Qian, Y., Y. Zheng, Y. Zhang, and M. Q. Miao, 2003: Responses of China's summer monsoon climate to snow anomaly over the Tibetan Plateau. *Int. J. Climatol.,* **23,** 593–613, doi:10.1002/joc.901.

Qiao, F., Z. Song, Y. Bao, Y. Song, Q. Shu, C. Huang, and W. Zhao, 2013: Development and evaluation of an Earth System Model with surface gravity waves. *J. Geophys. Res. Oceans,* **118,** 4514–4524, doi:10.1002/jgrc.20327.

Saha, S., and Coauthors, 2010: The NCEP Climate Forecast System Reanalysis. *Bull. Amer. Meteor. Soc.,* **91,** 1015–1057, doi:10.1175/2010BAMS3001.1.

Sakamoto, T. T., and Coauthors, 2012: MIROC4—A new high-resolution atmosphere–ocean coupled general circulation model. *J. Meteor. Soc. Japan,* **90,** 325–359, doi:10.2151/jmsj.2012-301.

Sarikaya, M. A., M. P. Bishop, J. F. Shroder, and J. A. Olsenholler, 2012: Space-based observations of Eastern Hindu Kush glaciers between 1976 and 2007, Afghanistan and Pakistan. *Remote Sens. Lett.,* **3,** 77–84, doi:10.1080/01431161.2010.536181.

Schmidt, G. A., and Coauthors, 2006: Present-day atmospheric simulations using GISS ModelE: Comparison to in situ, satellite, and reanalysis data. *J. Climate,* **19,** 153–192, doi:10.1175/JCLI3612.1.

Scoccimarro, E., and Coauthors, 2011: Effects of tropical cyclones on ocean heat transport in a high-resolution coupled general circulation model. *J. Climate,* **24,** 4368–4384, doi:10.1175/2011JCLI4104.1.

Singh, P., K. Ramasastri, and N. Kumar, 1995: Topographical influence on precipitation distribution in different ranges of Western Himalayas. *Nord. Hydrol.,* **26,** 259–284.

Sneyers, R., 1990: On the statistical analysis of series of observation. Tech. Note 143, WMO, 192 pp.

Su, F., X. Duan, D. Chen, Z. Hao, and L. Cuo, 2013: Evaluation of the global climate models in the CMIP5 over the Tibetan Plateau. *J. Climate,* **26,** 3187–3208, doi:10.1175/JCLI-D-12-00321.1.

Syed, F. S., F. Giorgi, J. S. Pal, and M. P. King, 2006: Effect of remote forcings on the winter precipitation of central southwest Asia part 1: Observations. *Theor. Appl. Climatol.,* **86,** 147–160, doi:10.1007/s00704-005-0217-1.

Tahir, A., P. Chevallier, Y. Arnaud, and B. Ahmad, 2011: Snow cover dynamics and hydrological regime of the Hunza River basin, Karakoram Range, northern Pakistan. *Hydrol. Earth Syst. Sci.,* **15,** 2275–2290, doi:10.5194/hess-15-2275-2011.

Tedesco, M., R. Kelly, J. Foster, and A. Chang, 2004: AMSR-E/*Aqua* Daily L3 global snow water equivalent EASE-Grids, version 2 [2002–2011]. National Snow and Ice Data Center, Boulder, CO, digital media. [Available online at http://nsidc.org/data/docs/daac/ae_swe_ease-grids.gd.html.]

van den Hurk, B. J., P. Viterbo, A. Beljaars, and A. Betts, 2000: Offline validation of the ERA40 surface scheme. Tech. Memo. 295, ECMWF, 42 pp. [Available online at www.knmi.nl/publications/fulltexts/tm295.pdf.]

Voldoire, A., and Coauthors, 2013: The CNRM-CM5.1 global climate model: Description and basic evaluation. *Climate Dyn.,* **40,** 2091–2121, doi:10.1007/s00382-011-1259-y.

Volodin, E., N. Dianskii, and A. Gusev, 2010: Simulating present-day climate with the INMCM4.0 coupled model of the atmospheric and oceanic general circulations. *Atmos. Oceanic Phys.,* **46,** 414–431, doi:10.1134/S000143381004002X.

Watanabe, M., and Coauthors, 2010: Improved climate simulation by MIROC5: Mean states, variability, and climate sensitivity. *J. Climate,* **23,** 6312–6335, doi:10.1175/2010JCLI3679.1.

Watanabe, S., and Coauthors, 2011: MIROC-ESM 2010: Model description and basic results of CMIP5-20c3m experiments. *Geosci. Model Dev.,* **4,** 845–872, doi:10.5194/gmd-4-845-2011.

Winiger, M., M. Gumpert, and H. Yamout, 2005: Karakorum–Hindukush–western Himalaya: Assessing high-altitude water resources. *Hydrol. Processes,* **19,** 2329–2338, doi:10.1002/hyp.5887.

Wu, T.-W., and Z.-A. Qian, 2003: The relation between the Tibetan winter snow and the Asian summer monsoon and rainfall: An observational investigation. *J. Climate,* **16,** 2038–2051, doi:10.1175/1520-0442(2003)016<2038:TRBTTW>2.0.CO;2.

——, and Coauthors, 2013: Global carbon budgets simulated by the Beijing Climate Center Climate System Model for the last century. *J. Geophys. Res. Atmos.,* **118,** 4326–4347, doi:10.1002/jgrd.50320.

Yao, T., J. Pu, A. Lu, Y. Wang, and W. Yu, 2007: Recent glacial retreat and its impact on hydrological processes on the Tibetan Plateau, China, and surrounding regions. *Arct. Antarct. Alp. Res.,* **39,** 642–650, doi:10.1657/1523-0430(07-510)[YAO]2.0.CO;2.

——, and Coauthors, 2012: Third Pole Environment (TPE). *Environ. Dev.,* **3,** 52–64, doi:10.1016/j.envdev.2012.04.002.

You, Q., S. Kang, G. Ren, K. Fraedrich, N. Pepin, Y. Yan, and L. Ma, 2011: Observed changes in snow depth and number of snow days in the eastern and central Tibetan Plateau. *Climate Res.,* **46,** 171–183, doi:10.3354/cr00985.

Yukimoto, S., Y. Adachi, and M. Hosaka, 2012: A new global climate model of the Meteorological Research Institute: MRI-CGCM3—Model description and basic performance. *J. Meteor. Soc. Japan,* **90A,** 23–64, doi:10.2151/jmsj.2012-A02.